

High-energy cLFV at μ TRISTAN: HNL extensions of the Standard Model

J. Kriewald ^a, E. Pinsard ^b and A. M. Teixeira ^c

^a Jožef Stefan Institut, Jamova Cesta 39, P. O. Box 3000, 1001 Ljubljana, Slovenia

^b Physik-Institut, Universität Zürich, CH-8057 Zürich, Switzerland

^c Laboratoire de Physique de Clermont Auvergne (UMR 6533), CNRS/IN2P3, Univ. Clermont Auvergne, 4 Av. Blaise Pascal, 63178 Aubière Cedex, France

Abstract

Within the context of heavy neutral lepton (HNL) extensions of the Standard Model, we compute the cross-sections for $\mu^+e^- \rightarrow \ell_\alpha^+\ell_\beta^-$ scattering, as well as several angular observables. In particular, we investigate the future sensitivity of a μ TRISTAN collider in discovering such charged lepton flavour violating processes and the potential constraining power of these searches on the parameter space of HNL models. Our results show that while low-energy probes of $\mu - e$ flavour violation do offer the most promising potential, the prospects for $e\tau$ and $\mu\tau$ flavour violation searches at μ TRISTAN can exceed those of related low-energy probes (as well as flavour violating Z -pole processes at FCC-ee) by several orders of magnitude.

1 Introduction

Heavy neutral leptons (HNL) are among the most appealing and yet most simple extensions of the Standard Model (SM). In particular, HNL (or heavy sterile fermions) are present in numerous extensions of the SM aiming at explaining neutrino mass generation: this is the case of minimal seesaw models, such as the type I [1–5], or variations of the latter, including realisations of the Linear Seesaw [6, 7], or of the Inverse Seesaw [8–10]. These heavy sterile states also emerge in the context of ambitious New Physics (NP) constructions, as for instance Left-Right symmetric extensions of the SM, or in Grand Unified Theories. Furthermore, their role in cosmology has also been intensively explored, as they might also play a role in explaining the observed baryon asymmetry of the Universe (via leptogenesis), or possibly account for (part) of the dark matter relic abundance.

In view of the manifest physics potential of these states, dedicated searches are being currently carried out, directly at the LHC, or indirectly via their role on a large number of high-intensity and/or electroweak precision observables. The physics cases and programmes of future colliders also prominently feature searches for these states.

Should the HNLs exhibit non-negligible couplings to the (light) active neutrinos, then they can also be at the source of significant contributions to charged lepton flavour violating (cLFV) decays and transitions: their role in low-energy cLFV processes has been extensively studied, be it in the framework of complete models, or then in minimal ad-hoc constructions, where the role of HNL is encoded in an enlarged spectrum and in new mixings to the active neutrinos [9, 11–30]. Searches for heavy sterile fermions at the high-energy frontier have also been intensively pursued in recent years: the physics programme of possible future colliders such as FCC-ee features numerous study cases, see e.g. [31–41] and references therein; likewise, searches for HNLs at a future Muon Collider have also been under recent scrutiny [42–49].

The case for an asymmetric electron-muon collider has also gained renewed momentum, in view of its potential as a uniquely powerful tool for cLFV searches, as well as precise measurements in the Higgs

sector. The asymmetric nature of the colliding beams substantially reduces (physics) backgrounds compared to both electron-positron or muon-antimuon collisions: for $e^-\mu^+$, SM-like final states mostly arise from higher order processes (including vector boson scattering and fusion). Such a facility - μ TRISTAN - has been proposed with several operating collision energies, possibly paving the way for a muon collider [50, 51]. As already discussed [52], an asymmetric collider would naturally offer the perfect testing grounds for (tree-level) flavour-violating new physics mediators, as is for instance the case of Z' models [53, 54] or flavour violating neutral and doubly charged scalars [55]. Likewise, the possibility of a same-sign lepton collider (e.g. $\mu^+\mu^+$) allows to resonantly probe lepton number violation (LN V) by two units (for example in processes such as $\mu^+\mu^+ \rightarrow W^+W^+ \rightarrow jjjj$ which can arise in different SM extensions encompassing a mechanism of Majorana neutrino mass generation). Singly or doubly resonant behaviour in m_{jj} or even m_{jjjj} then allows to distinguish different mediators and topologies, such as a doubly charged scalar in the s-channel or a heavy Majorana fermion mediator in a t-channel (see e.g. [55]). (Pseudo-) Observables constructed from event-shape variables of such scatterings offer probes of the neutrino nature, which are highly complementary to neutrinoless double beta decay (similar observables at hadron colliders have been recently studied in [56]).

In the framework of a minimal type I seesaw, a recent study has focussed on final states (signal and SM background) including charged leptons, missing energy (light neutrinos) and jets [57]; limits were inferred on active-sterile neutrino mixing angles, leading to new constraints potentially far stronger (two orders of magnitude) than those offered by studies of electroweak precision observables (EWPO).

In the present study we focus on the potential of an asymmetric electron-muon collider to search for heavy neutral leptons via (almost) background-free cLFV final state signatures. Albeit generating cLFV only at the 1-loop level, HNL with non-negligible couplings to active neutrinos can lead to a sizeable number of signal events. Interestingly, the underlying topologies offer a direct connection to low-energy cLFV observables, and/or to flavour violating $Z \rightarrow \ell_\alpha \ell_\beta$ (with $\alpha \neq \beta$) decays. Moreover, the asymmetric nature of the beams might be instrumental in probing the nature of the interaction at the source of the cLFV transition. In what follows, we thus consider all relevant topologies issuing from $\mu^+e^- \rightarrow \ell_\alpha^+\ell_\beta^-$ scatterings, including s- and t-channel penguin processes, as well as box diagrams. We offer a thorough description of the computation, and provide a number of useful expressions for future dedicated studies. In addition to the scattering cross-sections (leading to a very conservative estimation of the number of expected events), we also consider pseudo-rapidity distributions, and the forward-backward asymmetry, which - as we will subsequently discuss - offer additional insight onto the nature of the underlying processes.

Complementary to the μ TRISTAN observables mentioned above, we also consider a large number of low-energy cLFV transitions and decays (leptonic radiative and three-body decays, muon-electron conversion in nuclei and muonium oscillations) as well as cLFV Z boson decays, which can be searched for at the optimal environment of an FCC-ee in its Z -pole runs.

In order to illustrate the probing potential of μ TRISTAN in (indirect) cLFV searches for heavy neutral leptons, we consider a simplified NP model, in which two sterile states are added (in an ad-hoc manner) to the SM content; no assumption is made on the mechanism at the origin of the massive neutral lepton spectrum, the effect of the new heavy states being encoded in a generalised leptonic mixing matrix which extends the usual Pontecorvo–Maki–Nakagawa–Sakata (PMNS) matrix, U_{PMNS} . For completeness, we also study a UV-complete model of neutrino mass generation, which can be realised at low-energies without incurring in a loss of naturalness (in the sense of 't Hooft) - the Inverse Seesaw mechanism, specifically its (3,3) realisation, in which three generation of distinct species of HNL are added to the SM content. For both scenarios, we consider illustrative benchmark scenarios for spectrum and flavour patterns. In what concerns the nominal operating μ TRISTAN beam energies, several possibilities will be explored, leading to centre-of-mass (c.o.m.) energies from 100 GeV to 1100 GeV.

As we proceed to discuss, even for very conservative estimates of μ TRISTAN efficiency, one can expect a sizeable number of signal events while suppressing possible SM backgrounds to negligible rates: in particular, the t-channel dominated $\mu^+e^- \rightarrow \tau^+e^-$ and $\mu^+e^- \rightarrow \mu^+\tau^-$ scattering processes lead to tens or hundreds of thousands of events in large regions of the parameter space. We further point out that, should a $\mu^+e^- \rightarrow \ell_\alpha^+\ell_\alpha^-$ scattering process be discovered, measurements of the forward-

backward asymmetry of the final state leptons would grant access to further constrain the mass scale of the HNL via the interference of s- and t-channel contributions. (Notice that this interference behaviour can further be altered by the presence of additional CP-violating phases of the enlarged lepton mixing matrix.)

Finally, we analytically calculate the pseudo-rapidity distributions of the scattering cross-sections allowing to implement cuts in a straightforward manner. Based on these observations we suggest a basic and conservative “cut-and-count” analysis which allows us to estimate future sensitivities of a detector with ATLAS-like rapidity coverage to discover (or rather place bounds on) the high-energy cLFV observables.

In general, our findings suggest that while dedicated low-energy searches for $\mu - e$ flavour violation - in particular $\mu - e$ conversion in Nuclei - unquestionably offer the most promising probes for HNL at the origin of cLFV transitions, μ TRISTAN has a clear potential to outperform dedicated (low-energy) searches for $e\tau$ and $\mu\tau$ flavour violation - including Z -pole searches at FCC-ee.

The manuscript is organised as follows: we begin by a brief description of μ TRISTAN, focusing on its c.o.m. energies and expected luminosity. Section 3 is devoted to a detailed computation of high-energy observables which can be studied at μ TRISTAN. A brief description of the SM extensions via heavy sterile fermions here considered is offered in Section 4. Our results and discussion are presented in Section 5, followed by final remarks and prospective discussion. Additional (detailed and pedagogical) information outlining the calculation of the amplitudes is offered in several appendices.

2 An asymmetric lepton collider: μ TRISTAN

Recently, muon colliders have been the focus of intense discussion, as they would allow reaching higher energies than electron-positron colliders, offering also a much reduced expected background in comparison to pp colliders; if technically feasible, muon colliders could provide a perfect environment for successful direct searches for heavy new resonances and for impressive precision measurements. However, while the methods for achieving a focused and coherent μ^- beam are still under investigation, the technology to create low-emittance μ^+ beam, using ultra cold muons [58] is already established. Thus, relying on the technology developed for the muon $g - 2$ experiment at J-PARC [59], one can envisage a $\mu^+\mu^+$ as well as an asymmetric μ^+e^- collider - the two proposed configurations for μ TRISTAN. In the following we only focus on the asymmetric μ^+e^- mode, since the $\mu^+\mu^+$ configuration would have a much lower luminosity.

Assuming realistic operating parameters (see [50] for a 3 km ring design), one can expect that the instantaneous luminosity for the collisions, i.e.

$$\mathcal{L}_{\mu^+e^-}^{\text{inst}} = \frac{N_{\mu^+} N_{e^-}}{2\pi \sqrt{\sigma_{\mu^+x}^2 + \sigma_{e^-x}^2} \sqrt{\sigma_{\mu^+y}^2 + \sigma_{e^-y}^2}} \times f_{\text{rep}}, \quad (1)$$

in which f_{rep} denotes the collision frequency, N_ℓ the number of leptons per bunch and $\sigma_{\ell^\pm}^2$ the beams’ dimensions, might allow achieving $\mathcal{L}_{\mu^+e^-}^{\text{inst}} \sim \mathcal{O}(10^{34}) \text{cm}^{-2}\text{s}^{-1}$ [60–62], or even higher, for associated centre-of-mass energies ranging from a few hundred to a few thousand GeV. Nominal (E_{e^-}, E_{μ^+}) beam energies have been proposed, for example $(20 \text{ GeV}, 200 \text{ GeV})$, $(30 \text{ GeV}, 1 \text{ TeV})$, $(50 \text{ GeV}, 1 \text{ TeV})$ or $(100 \text{ GeV}, 3 \text{ TeV})$ [50, 51, 63] (see Table 1), which we will subsequently explore in our phenomenological discussion.

Even in the absence of a full knowledge of the accelerator characteristics, a realistic estimate of the instantaneous luminosity for μ TRISTAN in its $(30 \text{ GeV}, 1 \text{ TeV})$ configuration has been given in [50]; in what follows we rely on their result - $\mathcal{L}_{\text{inst}} = 4.6 \times 10^{33} \text{ cm}^{-2} \text{ s}^{-1}$ - thus leading to an integrated luminosity of 100 fb^{-1} per year and to a total integrated luminosity of 1 ab^{-1} after 10 years of data-taking.

3 High-energy cLFV observables at μ TRISTAN

The flavour-asymmetric colliding beams allow to investigate a number of processes for which there is no SM contribution. These include, firstly $\mu^+e^- \rightarrow \tau^+e^-$, relying on t-channel penguin processes (and

E_{e^-} (GeV)	E_{μ^+} (GeV)	\sqrt{s} (GeV)
20	200	126.5
30	1000	346.4
50	1000	447.2
100	3000	1095.4

Table 1: Different e^- and μ^+ beam energies considered, as well as the associated centre-of-mass energies.

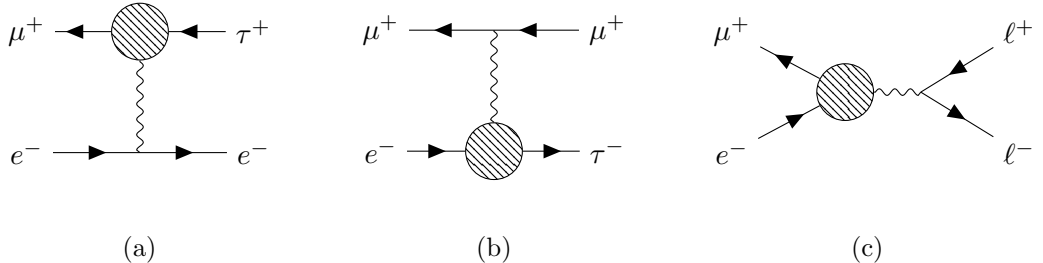


Figure 1: Feynman diagrams contributing to $\mu^+e^- \rightarrow \tau^+e^-$, $\mu^+e^- \rightarrow \mu^+\tau^-$ and $\mu^+e^- \rightarrow \ell^+\ell^-$. The shaded “blob” denotes the inclusion of the loop diagrams depicted in Fig. 2.

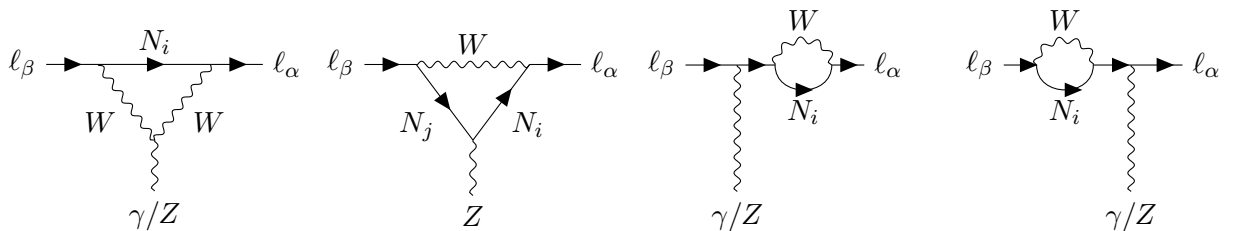


Figure 2: One-loop interactions contributing to the penguin-diagrams under consideration (see Fig. 1).

flavour violating corrections to the outgoing lepton propagators) as well as box diagrams, in which the electron acts as the “spectator flavour”. The contributing penguin diagrams are depicted in Fig. 1 (a). Secondly, one has $\mu^+e^- \rightarrow \mu^+\tau^-$, in full analogy to the previous case, but now with flavour violation occurring at the level of the electron line (spectator muon) (cf. Fig. 1 (b)). One also has $\mu^+e^- \rightarrow \tau^+\tau^-$ via s-channel and box diagrams, see Fig. 1 (c) for the corresponding penguin contributions. Finally, one has the very interesting $\mu^+e^- \rightarrow e^+\mu^-$, reflecting a double flavour violation, and which only occur via the box diagrams depicted in Fig. 3. The relevant Feynman rules for these interactions as well as the interaction Lagrangian are summarised in Appendix A.

From the topology of the flavour violating processes previously discussed, it is manifest that there is a clear connection with high-energy cLFV Z decays, and with several low-energy cLFV rare decays, including charged lepton radiative ($\ell_\alpha \rightarrow \ell_\beta \gamma$) and three-body ($\ell_\alpha \rightarrow \ell_\beta \ell_\delta \ell_\lambda$) decays, muonium oscillations as well as $\mu - e$ conversion - as we will further explore in subsequent sections.

As already mentioned, the amplitudes to the processes under consideration receive contributions from photon- and Z -penguins as well as box diagrams. Before entering the computation of the amplitudes, we note that in the limit of massless external fermions and once all Fierz transformations have been performed, the amplitudes admit only 3 types of Lorentz-structure:

$$\begin{aligned}
 \mathcal{M}_{LL} &= \mathcal{A}_{LL} [\bar{v}_\mu(p_1)\gamma^\mu P_L v_\alpha(p_3)] [\bar{u}_\beta(p_4)\gamma^\mu P_L u_e(p_2)], \\
 \mathcal{M}_{LR} &= \mathcal{A}_{LR} [\bar{v}_\mu(p_1)\gamma^\mu P_L v_\alpha(p_3)] [\bar{u}_\beta(p_4)\gamma^\mu P_R u_e(p_2)], \\
 \mathcal{M}_{RL} &= \mathcal{A}_{RL} [\bar{v}_\mu(p_1)\gamma^\mu P_R v_\alpha(p_3)] [\bar{u}_\beta(p_4)\gamma^\mu P_L u_e(p_2)],
 \end{aligned} \tag{2}$$

in which we chose the ordering of fermion fields as the reference order that all other fields will be Fierz-transformed into, with $\alpha, \beta = e, \mu, \tau$ depending on the given process. Squaring and spin-averaging the amplitude in the massless limit furthermore allows obtaining the differential cross-section as

$$\frac{d\sigma}{d \cos \theta} = \frac{1}{32\pi s} \left(|\mathcal{A}_{LL}|^2 u^2 + (|\mathcal{A}_{LR}|^2 + |\mathcal{A}_{RL}|^2) s^2 \right), \quad (3)$$

in which $\cos \theta = \frac{t-u}{s} = \frac{2t+s}{s}$ and s, t, u are the usual Mandelstam variables. Still in the massless limit, we have the following on-shell conditions

$$\begin{aligned} p_1^2 &= p_2^2 = p_3^2 = p_4^2 = 0, \\ (p_1 + p_2)^2 &= (p_3 + p_4)^2 = s, \\ (p_1 - p_3)^2 &= (p_4 - p_2)^2 = t, \\ (p_1 - p_4)^2 &= (p_4 - p_1)^2 = u, \\ s + t + u &= 0, \\ (p_1 p_2) &= (p_3 p_4) = \frac{s}{2}, \\ (p_1 p_3) &= (p_2 p_4) = -\frac{t}{2}, \\ (p_1 p_4) &= (p_2 p_3) = -\frac{u}{2}. \end{aligned} \quad (4)$$

For each of the purely leptonic processes the contributions to the amplitudes $\mathcal{A}_{LL,LR,RL}$ exhibit (slight) differences. We begin the discussion with the process $\mu^+ e^- \rightarrow \tau^+ e^-$, noticing that the expressions for the other processes can be obtained with the appropriate re-arrangements of flavour indices and squared momenta (crossing symmetry). We also stress that all diagrams have been computed in Feynman gauge¹.

In the massless limit, the amplitudes of the photon- and Z -penguins can be cast as

$$\mathcal{M}_\gamma = -g s_w Q_e \frac{1}{t} F_\gamma^{\mu\tau}(t) [\bar{v}_\mu(p_1) \gamma^\mu P_L v_\tau(p_3)] [\bar{u}_\beta(p_4) \gamma^\mu u_e(p_2)], \quad (5)$$

$$\mathcal{M}_Z = -\frac{g}{c_w} \frac{1}{t - m_Z^2} F_Z^{\mu\tau}(t) [\bar{v}_\mu(p_1) \gamma^\mu P_L v_\tau(p_3)] [\bar{u}_\beta(p_4) \gamma^\mu (g_V^e - g_A^e \gamma_5) u_e(p_2)], \quad (6)$$

in which $Q_e = -1$, the weak mixing angle encoded via $s_w, c_w = \sin \theta_w, \cos \theta_w$ (with $c_w = \frac{m_W}{m_Z}$ in the on-shell scheme), with the Z -couplings given as $g_V^f = \frac{1}{2} T_f^3 - Q_f \sin^2 \theta_w$ and $g_A^f = \frac{1}{2} T_f^3$. The form-factor $F_\gamma^{\alpha\beta}(q^2)$ can be written as

$$\begin{aligned} F_\gamma^{\alpha\beta}(q^2) &= -\frac{g^3 s_w}{32\pi^2 m_W^2} \sum_i \mathcal{U}_{\alpha i} \mathcal{U}_{\beta i}^* \left[(m_i^2 + (D-4)m_W^2) B_0 + (m_i^2 + (D-2)m_W^2) B_1 \right. \\ &\quad \left. + m_W^2 (2(m_i^2 - m_W^2) C_0 + q^2 (C_1 + C_2)) - 2(m_i^2 + (D-2)m_W^2) C_{00} \right], \end{aligned} \quad (7)$$

in which we abbreviated the Passarino-Veltman functions as $B_{0,1} \equiv B_{0,1}(0, m_i^2, m_W^2)$ and $C_{0,1,2,00} \equiv C_{0,1,2,00}(0, q^2, 0, m_i^2, m_W^2, m_W^2)$, in the convention of LoopTools [64]; $D = 4 - 2\epsilon$ is the dimensionality of space-time. Furthermore, \mathcal{U} denotes the extended lepton mixing matrix (see also Appendix A). The squared vector-momentum q^2 has to be replaced with one of the Mandelstam variables s, t, u , depending on the process under consideration. For $\mu^+ e^- \rightarrow \tau^+ e^-$ we have $q^2 = t$. Furthermore, the index i runs over the internal neutrino states, while α, β are the charged lepton flavours (i.e. $\alpha = \mu$ and $\beta = \tau$ for $\mu^+ e^- \rightarrow \tau^+ e^-$). The form-factor of the Z -penguin $F_Z^{\alpha\beta}(q^2)$ is more involved and, for convenience, it is split into

$$F_Z^{\alpha\beta}(q^2) = G_Z^{\alpha\beta}(q^2) + H_Z^{\alpha\beta}(q^2), \quad (8)$$

¹Whilst the corresponding diagrams with Goldstone modes have been omitted from our figures, they are naturally included in our calculations.

with

$$\begin{aligned}
G_Z^{\alpha\beta}(q^2) &= \frac{g^3}{32\pi^2 c_w m_W^2} \sum_i \mathcal{U}_{\alpha i} \mathcal{U}_{\beta i}^* \left[2c_w^2 m_W^2 B_0 + (g_V^\ell + g_A^\ell)(m_i^2 + (D-2)m_W^2)(B_0 + B_1) \right. \\
&\quad + c_w m_W (2(s_w^2 m_i^2 m_Z + c_w m_W^3) C_0 - c_w m_W q^2 (C_1 + C_2) \\
&\quad \left. - ((2c_w^2 - 1)m_i^2 + 2c_w^2 (D-2)m_W^2) C_{00} \right], \tag{9}
\end{aligned}$$

in which the Passarino-Veltman functions correspond to $B_{0,1} \equiv B_{0,1}(0, m_i^2, m_W^2)$ and $C_{0,1,2,00} \equiv C_{0,1,2,00}(0, q^2, 0, m_i^2, m_W^2, m_j^2)$. The second term is given by

$$\begin{aligned}
H_Z^{\alpha\beta}(q^2) &= \frac{g^3}{64\pi^2 c_w m_W^2} \sum_{i,j} \mathcal{U}_{\alpha i} \mathcal{U}_{\beta j}^* \left\{ \mathcal{C}_{ij} \left[m_W^2 ((6-D)B_0^{ij} - 2B_0^i - 2B_0^j \right. \right. \\
&\quad - (2m_i^2 + 2m_j^2 + (D-6)m_W^2 - 2q^2) C_0 + 2(D-2) C_{00} + m_i^2 m_j^2 C_0 \\
&\quad \left. \left. + \mathcal{C}_{ij}^* m_i m_j \left[B_0^{ij} - (D-3)m_W^2 C_0 - 2C_{00} \right] \right] \right\}, \tag{10}
\end{aligned}$$

in which $B_0^{i,j} \equiv B_0(0, m_W^2, m_i^2)$, $B_0^{ij} \equiv B_0(q^2, m_i^2, m_j^2)$, and $C_{0,00} \equiv C_{0,00}(0, q^2, 0, m_W^2, m_i^2, m_j^2)$ denote the compact version of the Passarino-Veltman functions. For the definition of \mathcal{C} , see Eq. (60).

Before proceeding to the box diagrams, let us stress here that while the $B_{0,1}$ - and C_{00} -functions have divergent terms, their combinations entering in the full loop-functions are finite due to (semi-) unitarity of the lepton mixing matrix \mathcal{U} . For more details on the finiteness of the Z -penguin, see also the related discussion in [65]. Furthermore, we emphasise that the Z -penguin amplitude is only gauge-invariant for an on-shell Z , which is clearly not the case here. Only upon inclusion of the corresponding photon-penguin as well as the box diagrams, is gauge-invariance restored in the full amplitude. (This can be checked via an explicit computation of the process in the R_ξ -gauge, leading to extremely lengthy (analytical) expressions which we refrain from reproducing here.) For a related discussion see e.g. [66].

While the computation of the penguin contributions is tedious but fairly straightforward, the computation of the box-diagrams contains several less trivial steps which are outlined in more detail in Appendix B. Here, we just give the main results necessary to numerically evaluate the amplitude. The four box diagrams shown in Figure 3 contribute to $\mu^+ e^- \rightarrow \ell_\alpha^+ \ell_\beta^-$ processes. We notice here that the upper row contains only Lepton Number conserving interactions while the lower row also contains LNV interactions or, more broadly speaking, fermion number violating vertices. The derivation of the Feynman rules for these vertices are taken from [67] and summarised in Appendix A.

The four box contributions to the amplitude for $\mu^+ e^- \rightarrow \ell_\alpha^+ \ell_\beta^-$ (following the labelling of Figure 3) can be written in the massless limit as

$$\mathcal{M}_1 = \mathcal{B}_1^{\alpha\beta}(t, s) [\bar{v}_\mu(p_1) \gamma^\mu P_L u_e(p_2)] [\bar{u}_\beta(p_4) \gamma^\mu P_L v_\alpha(p_3)], \tag{11}$$

$$\mathcal{M}_2 = \mathcal{B}_2^{\alpha\beta}(s, t) [\bar{v}_\mu(p_1) \gamma^\mu P_L v_\alpha(p_3)] [\bar{u}_\beta(p_4) \gamma^\mu P_L u_e(p_2)], \tag{12}$$

$$\mathcal{M}_3 = \mathcal{B}_3^{\alpha\beta}(s, u) [\bar{v}_\mu(p_1) P_R v_\beta(p_4)] [\bar{u}_\alpha(p_3) P_L u_e(p_2)], \tag{13}$$

$$\mathcal{M}_4 = \mathcal{B}_4^{\alpha\beta}(t, u) [\bar{v}_\mu(p_1) P_R v_\beta(p_4)] [\bar{u}_\alpha(p_3) P_L u_e(p_2)]. \tag{14}$$

Clearly, the four-fermion structures appearing in \mathcal{M}_1 , \mathcal{M}_3 and \mathcal{M}_4 have to be Fierz-transformed to the reference order of the penguins, which coincides with the ordering of \mathcal{M}_2 . Making use of the Fierz identities derived in [68], one can show that

$$[\bar{v}_\mu(p_1) \gamma^\mu P_L u_e(p_2)] [\bar{u}_\beta(p_4) \gamma^\mu P_L v_\alpha(p_3)] = [\bar{v}_\mu(p_1) \gamma^\mu P_L v_\alpha(p_3)] [\bar{u}_\beta(p_4) \gamma^\mu P_L u_e(p_2)], \tag{15}$$

$$[\bar{v}_\mu(p_1) P_R v_\beta(p_4)] [\bar{u}_\alpha(p_3) P_L u_e(p_2)] = -\frac{1}{2} [\bar{v}_\mu(p_1) \gamma^\mu P_L v_\alpha(p_3)] [\bar{u}_\beta(p_4) \gamma^\mu P_L u_e(p_2)]. \tag{16}$$

The various box form-factors and their loop-functions can be written as

$$\mathcal{B}_1^{\alpha\beta}(t, s) = \frac{g^4}{128\pi^2} \sum_{i,j} \mathcal{U}_{\alpha i}^* \mathcal{U}_{\beta j} \mathcal{U}_{ei}^* \mathcal{U}_{\mu i} F_1(t, s), \tag{17}$$

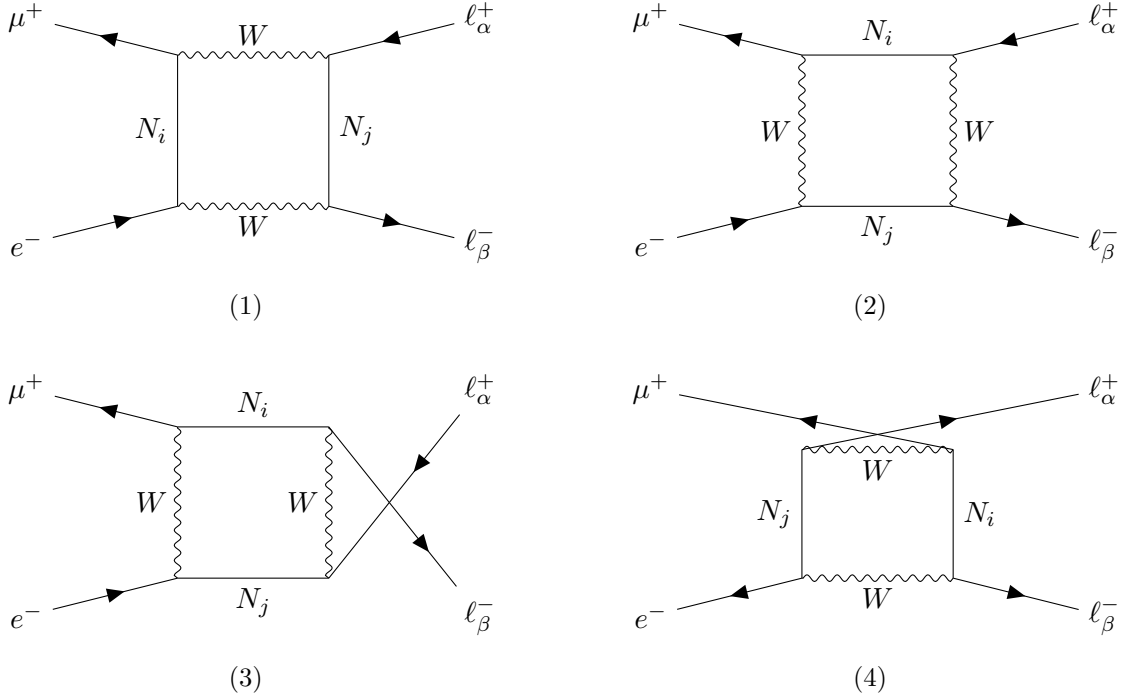


Figure 3: Box diagrams contributing to $\mu^+ e^- \rightarrow \ell_\alpha^+ \ell_\beta^-$. The upper row only contains lepton number conserving interactions, while the lower row also contains lepton violating vertices.

$$\mathcal{B}_2^{\alpha\beta}(s, t) = \frac{g^4}{128\pi^2} \sum_{i,j} \mathcal{U}_{\alpha i}^* \mathcal{U}_{\beta j} \mathcal{U}_{ej}^* \mathcal{U}_{\mu i} F_1(s, t), \quad (18)$$

$$\mathcal{B}_3^{\alpha\beta}(s, u) = \frac{g^4}{64\pi^2} \sum_{i,j} \mathcal{U}_{\alpha j}^* \mathcal{U}_{\beta i} \mathcal{U}_{ej}^* \mathcal{U}_{\mu i} F_2(s, u), \quad (19)$$

$$\mathcal{B}_4^{\alpha\beta}(t, u) = \frac{g^4}{64\pi^2} \sum_{i,j} \mathcal{U}_{\alpha j}^* \mathcal{U}_{\beta i} \mathcal{U}_{ej}^* \mathcal{U}_{\mu i} F_2(t, u), \quad (20)$$

$$\begin{aligned} F_1(q_1^2, q_2^2) = & \frac{1}{m_W^4} \left(q_1^2 (m_i^2 m_j^2 + 4m_W^4) (D_1 + D_{11} + D_{12} + D_{13}) \right. \\ & \left. + 4m_W^4 q_1^2 (D_2 + D_3) - 4m_i^2 m_j^2 m_W^2 D_0 + 2(m_i^2 m_j^2 + 4m_W^4) D_{00} \right), \end{aligned} \quad (21)$$

$$\begin{aligned} F_2(q_1^2, q_2^2) = & \frac{m_i m_j}{m_W^4} \left((m_i^2 m_j^2 + 4m_W^4) D_0 - 2m_W^2 \left(4D_{00} \right. \right. \\ & \left. \left. + 2q_1^2 (D_1 + D_{11} + D_{12} + D_{13} + D_{23} + \frac{D_2 + D_3}{2}) \right) \right), \end{aligned} \quad (22)$$

in which the Passarino-Veltman four-point functions (in the LoopTools [64] convention) were introduced as $D_{ij} \equiv D_{ij}(q_1^2, 0, q_2^2, 0, 0, 0, m_i^2, m_j^2, m_W^2, m_W^2)$. We note that the four-point functions are all finite.

We are now able to bring together all contributions to the amplitudes defined in (2). For the process $\mu^+ e^- \rightarrow \tau^+ e^-$ they are obtained in a straightforward manner from the penguins and boxes: making use of the Fierz rearrangements in Eq. (15) and (16), as

$$\mathcal{A}_{LL}^{\mu e \tau e} = \mathcal{B}_1^{\tau e}(t, s) + \mathcal{B}_2^{\tau e}(s, t) - \frac{\mathcal{B}_3^{\tau e}(s, u) + \mathcal{B}_4^{\tau e}(t, u)}{2} - \frac{g}{c_w} \frac{g_V^e + g_A^e}{t - m_Z^2} F_Z^{\mu \tau}(t) - \frac{g s_w Q_e}{t} F_\gamma^{\mu \tau}(t), \quad (23)$$

$$\mathcal{A}_{LR}^{\mu e \tau e} = -\frac{g}{c_w} \frac{g_V^e - g_A^e}{t - m_Z^2} F_Z^{\mu \tau}(t) - \frac{g s_w Q_e}{t} F_\gamma^{\mu \tau}(t), \quad (24)$$

$$\mathcal{A}_{RL}^{\mu e \tau e} = 0. \quad (25)$$

For the other processes, the corresponding expressions can be derived simply by appropriately re-arranging flavour indices and momentum transfers. For $\mu^+e^- \rightarrow \mu^+\tau^-$ we have the same box-contributions but with the exchange $\tau \leftrightarrow e$ indices, while the penguin contributions require more work. Instead of having the flavour violating penguin insertion in the muon line (see diagram (a) in Figure 1), it now appears in the electron line (see Figure 1 (b)); after some algebra this leads to

$$\mathcal{A}_{LL}^{\mu e \mu \tau} = \mathcal{B}_1^{e\tau}(t, s) + \mathcal{B}_2^{e\tau}(s, t) - \frac{\mathcal{B}_3^{e\tau}(s, u) + \mathcal{B}_4^{e\tau}(t, u)}{2} - \frac{g}{c_w} \frac{g_V^\mu + g_A^\mu}{t - m_Z^2} F_Z^{\tau e}(t) - \frac{g s_w Q_\mu}{t} F_\gamma^{\tau e}(t), \quad (26)$$

$$\mathcal{A}_{LR}^{\mu e \mu \tau} = 0, \quad (27)$$

$$\mathcal{A}_{RL}^{\mu e \mu \tau} = -\frac{g}{c_w} \frac{g_V^\mu - g_A^\mu}{t - m_Z^2} F_Z^{\tau e}(t) - \frac{g s_w Q_\mu}{t} F_\gamma^{\tau e}(t). \quad (28)$$

For the third case of $\mu^+e^- \rightarrow \ell^+\ell^-$ pair-production, we need to distinguish 3 sub-cases depending on final state flavours. In addition to the t-channel like penguin contributions we also have now annihilation s-channel like penguins (see diagram (c) of Figure 1). These lead to different four-fermion structures which can however be easily Fierz-rearranged into the reference order via Eq. (15) and Eq. (16). The amplitudes consequently receive contributions from the boxes, s-channel penguins and in the cases of $\ell = e(\mu)$ also “upper” (“lower”) t-channel penguins. These are given by

$$\mathcal{A}_{LL}^{\mu e e e} = \mathcal{B}_1^{ee}(t, s) + \mathcal{B}_2^{ee}(s, t) - \frac{\mathcal{B}_3^{ee}(s, u) + \mathcal{B}_4^{ee}(t, u)}{2} - \frac{g}{c_w} \frac{g_V^e + g_A^e}{t - m_Z^2} F_Z^{\mu e}(t) - \frac{g s_w Q_e}{t} F_\gamma^{\mu e}(t) - \frac{g}{c_w} \frac{g_V^e + g_A^e}{s - m_Z^2} F_Z^{\mu e}(s) - \frac{g s_w Q_e}{s} F_\gamma^{\mu e}(s), \quad (29)$$

$$\mathcal{A}_{LR}^{\mu e e e} = -\frac{g}{c_w} \frac{g_V^e - g_A^e}{t - m_Z^2} F_Z^{\mu e}(t) - \frac{g s_w Q_e}{t} F_\gamma^{\mu e}(t) - \frac{g}{c_w} \frac{g_V^e - g_A^e}{s - m_Z^2} F_Z^{\mu e}(s) - \frac{g s_w Q_e}{s} F_\gamma^{\mu e}(s), \quad (30)$$

$$\mathcal{A}_{RL}^{\mu e e e} = 0, \quad (31)$$

$$\mathcal{A}_{LL}^{\mu e \mu \mu} = \mathcal{B}_1^{\mu\mu}(t, s) + \mathcal{B}_2^{\mu\mu}(s, t) - \frac{\mathcal{B}_3^{\mu\mu}(s, u) + \mathcal{B}_4^{\mu\mu}(t, u)}{2} - \frac{g}{c_w} \frac{g_V^\mu + g_A^\mu}{t - m_Z^2} F_Z^{\mu e}(t) - \frac{g s_w Q_\mu}{t} F_\gamma^{\mu e}(t) - \frac{g}{c_w} \frac{g_V^\mu + g_A^\mu}{s - m_Z^2} F_Z^{\mu e}(s) - \frac{g s_w Q_\mu}{s} F_\gamma^{\mu e}(s), \quad (32)$$

$$\mathcal{A}_{LR}^{\mu e \mu \mu} = -\frac{g}{c_w} \frac{g_V^\mu - g_A^\mu}{s - m_Z^2} F_Z^{\mu e}(s) - \frac{g s_w Q_\mu}{s} F_\gamma^{\mu e}(s), \quad (33)$$

$$\mathcal{A}_{RL}^{\mu e \mu \mu} = -\frac{g}{c_w} \frac{g_V^\mu - g_A^\mu}{t - m_Z^2} F_Z^{\mu e}(t) - \frac{g s_w Q_\mu}{t} F_\gamma^{\mu e}(t), \quad (34)$$

$$\mathcal{A}_{LL}^{\mu e \tau \tau} = \mathcal{B}_1^{\tau\tau}(t, s) + \mathcal{B}_2^{\tau\tau}(s, t) - \frac{\mathcal{B}_3^{\tau\tau}(s, u) + \mathcal{B}_4^{\tau\tau}(t, u)}{2} - \frac{g}{c_w} \frac{g_V^\tau + g_A^\tau}{s - m_Z^2} F_Z^{\mu e}(s) - \frac{g s_w Q_\tau}{s} F_\gamma^{\mu e}(s) \quad (35)$$

$$\mathcal{A}_{LR}^{\mu e \tau \tau} = -\frac{g}{c_w} \frac{g_V^\tau - g_A^\tau}{s - m_Z^2} F_Z^{\mu e}(s) - \frac{g s_w Q_\tau}{s} F_\gamma^{\mu e}(s), \quad (36)$$

$$\mathcal{A}_{RL}^{\mu e \tau \tau} = 0. \quad (37)$$

Lastly, we have the high-energy equivalent of muonium-antimuonium oscillation, namely $\mu^+e^- \rightarrow e^+\mu^-$. Just like its low-energy counterpart, it is only mediated by box diagrams and thus we have

$$\mathcal{A}_{LL}^{\mu e e \mu} = \mathcal{B}_1^{e\mu}(t, s) + \mathcal{B}_2^{e\mu}(s, t) - \frac{\mathcal{B}_3^{e\mu}(s, u) + \mathcal{B}_4^{e\mu}(t, u)}{2}, \quad (38)$$

$$\mathcal{A}_{LR}^{\mu e e \mu} = \mathcal{A}_{RL}^{\mu e e \mu} = 0. \quad (39)$$

4 Theoretical frameworks and experimental constraints

As discussed in the Introduction, heavy sterile states are naturally present in numerous well-motivated models of New Physics, especially those aiming at addressing neutrino mass generation. Many such

Beyond the Standard Model (BSM) realisations offer rich phenomenological signatures, which in turn lead to extensive constraints on these new states. Below we briefly describe the theoretical frameworks upon which we will rely for our studies, also summarising the most pertinent constraints (phenomenological and experimental) on heavy neutral leptons.

4.1 SM extensions via HNL

As mentioned before, in order to illustrate the most relevant aspects of our study, we choose to consider two SM extensions featuring HNL: a minimal “3+2” construction and a realisation of the Inverse Seesaw, the ISS(3,3).

Ad-hoc minimal construction A possible approach to study the role of HNL in cLFV processes consists in considering minimal extensions of the SM, in which n_S sterile states are added to the particle content. Other than assuming that these heavy neutral fermions are massive (and of Majorana nature), and that they do have non-negligible mixings to the active neutrinos, no other hypothesis is made, in particular concerning their contribution to the mechanism of neutrino mass generation. In these minimal “ad-hoc” models the (generalised) leptonic mixings are thus encoded in a $(3 + n_S) \times (3 + n_S)$ unitary mixing matrix, \mathcal{U} ; its upper left 3×3 block corresponds to the left-handed leptonic mixing matrix (the would-be PMNS, \tilde{U}_{PMNS}) - no longer unitary.

In what follows we will consider the case of $n_S = 2$: the neutral lepton spectrum is thus composed of three light and 2 heavy mass eigenstates (m_i , with $i = 1 \dots 5$); the 5×5 unitary leptonic mixing matrix can be parametrised via ten angles (through subsequent rotations, also comprising 6 Dirac phases) and a diagonal matrix including four physical Majorana phases (cf. [69, 70]).

The enlarged lepton mixing matrix \mathcal{U} can be parametrised in the Euler representation via ten subsequent rotations R_{ij} (with $i \neq j$), multiplied with a diagonal matrix including the four physical Majorana phases φ_i

$$\mathcal{U} = R_{45} R_{35} R_{25} R_{15} R_{34} R_{24} R_{14} R_{23} R_{13} R_{12} \times \text{diag}(1, e^{i\varphi_2}, e^{i\varphi_3}, e^{i\varphi_4}, e^{i\varphi_5}). \quad (40)$$

The rotations around the Euler angles are given by (illustrated by R_{24}):

$$R_{24} = \begin{pmatrix} 1 & 0 & 0 & 0 & 0 \\ 0 & \cos \theta_{24} & 0 & \sin \theta_{24} e^{-i\delta_{24}} & 0 \\ 0 & 0 & 1 & 0 & 0 \\ 0 & -\sin \theta_{24} e^{-i\delta_{24}} & 0 & \cos \theta_{24} & 0 \\ 0 & 0 & 0 & 0 & 1 \end{pmatrix}. \quad (41)$$

We further note that the angles of the first three rotations (R_{12} , R_{13} and R_{23}) are fixed by neutrino oscillation data [71]. Finally, one has to choose 6 independent linear combinations of the ten “Dirac-like” CP phases present in the rotation matrices as physical.

A simple Inverse Seesaw realisation The Inverse Seesaw constitutes a variant of the type I seesaw which allows for a natural explanation of the smallness of the observed neutrino masses. It relies on the introduction of two species of sterile fermions, X and ν_R . The new terms at the origin of neutrino mass generation can be cast as

$$\mathcal{L}_{\text{ISS}} = -Y_{ij}^D \overline{L}_i^c \tilde{H} \nu_{Rj}^c - M_R^{ij} \overline{\nu}_{Ri} X_j - \frac{1}{2} \mu_R^{ij} \overline{\nu}_{Ri}^c \nu_{Rj} - \frac{1}{2} \mu_X^{ij} \overline{X}_i^c X_j + \text{H.c.} \quad (42)$$

Notice that upon $\mu_{X,R} \rightarrow 0$, one recovers total lepton number conservation. In the limit of approximate lepton number conservation, and taking for simplicity $\mu_R \rightarrow 0$ i.e. $\mu_X \ll m_D \ll M_R$, the masses of the light neutrinos are, to a good approximation², given by

$$m_\nu \simeq m_D \left(M_R^{-1} \right)^T \mu_X M_R^{-1} m_D^T \equiv U_{\text{PMNS}}^* m_\nu^{\text{diag}} U_{\text{PMNS}}^\dagger. \quad (43)$$

²Notice that μ_R only appears at higher orders in the seesaw expansion in the active neutrino mass and can therefore be safely neglected, see for example [72].

As can be seen from the above expression, the limit $\mu_X \rightarrow 0$ (and hence the generation of small neutrino masses for not excessively heavy M_R) becomes natural in the sense of 't Hooft [73, 74], since for $\mu_X = 0$ lepton number is restored.

In what follows we will consider a simple realisation of the ISS in which $n_R = n_X = 3$ generations of heavy sterile fermions are added to SM particle content, the so-called ISS(3,3)³.

As frequently done upon phenomenological studies of BSM scenarios of neutrino mass generation, it proves convenient and useful to consider parametrisations of the flavour structures of the model. For the ISS, a possibility consists in a modified Casas-Ibarra parametrisation [76],

$$m_D^T = V^\dagger \sqrt{M^{\text{diag}}} R \sqrt{m_\nu^{\text{diag}}} U_{\text{PMNS}}^\dagger, \quad (44)$$

in which the Dirac mass term (or equivalently the Yukawa couplings) encodes neutrino data, with the additional degrees of freedom parametrised via a complex orthogonal matrix R ; in the above equation, the unitary matrix V diagonalises M as $M = V^\dagger M^{\text{diag}} V^*$, and R can be parametrised as

$$R = \begin{pmatrix} c_2 c_3 & -c_1 s_3 - s_1 s_2 c_3 & s_1 s_3 - c_1 s_2 c_3 \\ c_2 s_3 & c_1 c_3 - s_1 s_2 s_3 & -s_1 c_3 - c_1 s_2 s_3 \\ s_2 & s_1 c_2 & c_1 c_2 \end{pmatrix}, \quad (45)$$

in which $s_i \equiv \sin \theta_i$, $c_i \equiv \cos \theta_i$ and $\theta_i \in \mathbb{C}$.

4.2 Constraints on heavy neutral leptons

In association with the potentially light new states, the above described modified currents open the door to contributions to numerous observables, ranging from flavoured transitions (including cLFV observables), to electroweak precision observables, among others. Likewise, neutrino oscillation data are also taken into account (using the recent results of NuFit6.0 [71]).

Phenomenological constraints: perturbative unitarity Bounds on the width of the heavy states can be inferred from constraints arising from perturbative unitarity⁴ [78–82]:

$$\frac{\Gamma(N_i)}{m_{N_i}} < \frac{1}{2}, \quad \text{for } i \geq 4; \quad (46)$$

for an HNL spectrum considerably heavier than all SM states (as is our case), the leading contributions to the HNL decay width arise from the two-body decays into a SM boson and a lepton. At tree level, these are given by (see, e.g. [83])

$$\Gamma(N_i \rightarrow W l_\alpha) = \frac{g_w^2}{64\pi} |\mathcal{U}_{\alpha i}|^2 \frac{\lambda^{1/2}(m_i^2, M_W^2, m_{l_\alpha}^2)}{m_i} \left\{ 1 + \frac{m_{l_\alpha}^2 - 2M_W^2}{m_i^2} + \frac{(m_i^2 - m_{l_\alpha}^2)^2}{m_i^2 M_W^2} \right\}, \quad (47)$$

$$\Gamma(N_i \rightarrow Z N_j) = \frac{g_w^2}{128 c_w^2 \pi} |C_{ij}|^2 \frac{\lambda^{1/2}(m_i^2, M_Z^2, m_j^2)}{m_i} \left\{ 1 + \frac{m_j^2 - 2M_Z^2}{m_i^2} + \frac{(m_i^2 - m_j^2)^2}{m_i^2 M_Z^2} \right\}, \quad (48)$$

$$\Gamma(N_i \rightarrow H N_j) = \frac{g_w^2}{128\pi} |C_{ij}|^2 \frac{m_i^2}{M_W^2} \frac{\lambda^{1/2}(m_i^2, M_H^2, m_j^2)}{m_i} \left\{ \left(1 + \frac{m_j^2 - M_H^2}{m_i^2} \right) \left(1 + \frac{m_j^2}{m_i^2} \right) + 4 \frac{m_j^2}{m_i^2} \right\}, \quad (49)$$

in which $\lambda(a, b, c) = [a - (\sqrt{b} - \sqrt{c})^2] [a - (\sqrt{b} + \sqrt{c})^2]$ is the Källén function. In turn, the constraints on the HNL decay width will have an impact on the allowed parameter space of the considered theoretical framework.

³For a detailed discussion of the most minimal ISS realisations, see [75].

⁴For a recent explicit computation of all relevant partial wave amplitudes in the $2 \rightarrow 2$ -scatterings see [77].

A non-unitary leptonic mixing matrix The deviations of the U_{PMNS} from unitarity (induced by the mixings between active and sterile neutral fermions) are at the origin of deviations from the SM expectations - concerning both flavour violating and flavour conserving leptonic transitions. The so-called η -matrix, defined as [84]

$$U_{\text{PMNS}} \rightarrow \tilde{U}_{\text{PMNS}} = (1 - \eta) U_{\text{PMNS}}, \quad (50)$$

proves convenient to evaluate deviations of U_{PMNS} from unitarity. Comprehensive analyses have allowed to infer constraints on the entries of η [83, 85–87], stemming from a number of flavour observables and electroweak precision tests: these include oblique parameters, the invisible width of the Z boson, muon decays, among others. Since these observables lead to subdominant constraints in the numerical analysis, we will not discuss them in detail, rather focusing on the new contributions to flavoured observables.

Flavoured observables: charged lepton flavour violation and lepton flavour universality
 In general, constraints from the non-observation of rare cLFV transitions and decays are at origin of the strongest bounds on SM extensions via HNL states. Among the most important modes one has cLFV three-body decays, $\mu - e$ conversion in muonic atoms, as well as cLFV Z boson decays. The bounds and future sensitivities concerning the decays which will be considered in our study are summarised in Table 2. In the context of SM extensions via n_S generations of HNL, the expressions for the cLFV observables can be found, for example, in [9, 11–20, 22–25, 27, 28, 88].

Observable	Current bound	Future sensitivity
$\text{BR}(\mu \rightarrow e\gamma)$	$< 3.1 \times 10^{-13}$ (MEG II [89])	6×10^{-14} (MEG II [90])
$\text{BR}(\tau \rightarrow e\gamma)$	$< 3.3 \times 10^{-8}$ (BaBar [91])	3×10^{-9} (Belle II [92])
$\text{BR}(\tau \rightarrow \mu\gamma)$	$< 4.2 \times 10^{-8}$ (Belle [93])	10^{-9} (Belle II [92])
$\text{BR}(\mu \rightarrow 3e)$	$< 1.0 \times 10^{-12}$ (SINDRUM [94])	$10^{-15(-16)}$ (Mu3e [95])
$\text{BR}(\tau \rightarrow 3e)$	$< 2.7 \times 10^{-8}$ (Belle [96])	5×10^{-10} (Belle II [92])
$\text{BR}(\tau \rightarrow 3\mu)$	$< 1.9 \times 10^{-8}$ (Belle II [97])	5×10^{-10} (Belle II [92])
$\text{BR}(\tau^- \rightarrow e^- \mu^+ \mu^-)$	$< 2.7 \times 10^{-8}$ (Belle [96])	5×10^{-10} (Belle II [92])
$\text{BR}(\tau^- \rightarrow \mu^- e^+ e^-)$	$< 1.8 \times 10^{-8}$ (Belle [96])	5×10^{-10} (Belle II [92])
$\text{BR}(\tau^- \rightarrow e^- \mu^+ e^-)$	$< 1.5 \times 10^{-8}$ (Belle [96])	3×10^{-10} (Belle II [92])
$\text{BR}(\tau^- \rightarrow \mu^- e^+ \mu^-)$	$< 1.7 \times 10^{-8}$ (Belle [96])	4×10^{-10} (Belle II [92])
$\text{CR}(\mu - e, N)$	$< 7 \times 10^{-13}$ (Au, SINDRUM [99])	10^{-14} (SiC, DeeMe [100]) 2.6×10^{-17} (Al, COMET [101–103]) 8×10^{-17} (Al, Mu2e [104])
$\text{P}(\text{Mu}-\overline{\text{Mu}})$	$< 8.3 \times 10^{-11}$ (PSI [105])	$\mathcal{O}(10^{-13})$ (MACE [106])
$\text{BR}(Z \rightarrow e^\pm \mu^\mp)$	$< 4.2 \times 10^{-7}$ (ATLAS [107])	$\mathcal{O}(10^{-10})$ (FCC-ee [98])
$\text{BR}(Z \rightarrow e^\pm \tau^\mp)$	$< 4.1 \times 10^{-6}$ (ATLAS [108])	$\mathcal{O}(10^{-10})$ (FCC-ee [98])
$\text{BR}(Z \rightarrow \mu^\pm \tau^\mp)$	$< 5.3 \times 10^{-6}$ (ATLAS [108])	$\mathcal{O}(10^{-10})$ (FCC-ee [98])

Table 2: Current experimental bounds and future sensitivities on relevant cLFV observables. The quoted limits are given at 90% C.L. (Belle II sensitivities correspond to an integrated luminosity of 50 ab^{-1} .)

The modified charged and neutral currents (a direct consequence of the non-unitarity of the PMNS mixing matrix) also has non-negligible consequences for (flavoured) universality ratios. This is the case for leptonic decays of light mesons - such as kaons and pions (see, for example [109, 110]), as well as tau-lepton decays from the comparison of the widths $\Gamma(\tau \rightarrow \mu\nu\nu)$ and $\Gamma(\tau \rightarrow e\nu\nu)$ (i.e. the R_τ ratio). Likewise, and at the frontier with EWPO, one also must also take into account lepton flavour

universality tests in Z boson decays, $\Gamma(Z \rightarrow \ell_\alpha \ell_\alpha)$ and $\Gamma(Z \rightarrow \ell_\beta \ell_\beta)$, or equivalently $R_{\alpha\beta}^Z$. We have addressed these observables within the framework of the ISS(3,3) in a recent study [83].

5 Results

We proceed to discuss the most important points of our analysis, numerically assessing the comparative prospects of observing cLFV $2 \rightarrow 2$ scatterings at μ TRISTAN, in view of other cLFV constraints (arising from low-energy searches and Z decays). As already mentioned, we will also evaluate angular distributions. Our study relies on several beam configurations (cf. Table 1), and we do not take into account the possibility of beam polarisation. Finally we will comment on the unique power of μ TRISTAN to probe $\mu - \tau$ sector flavour violation.

We illustrate most of our results relying (for simplicity) on the minimal ad-hoc SM extension; we conclude our study by evaluating the prospects of μ TRISTAN regarding the ISS(3,3).

5.1 General prospects: “3+2” ad-hoc extension

To illustrate the prospects of this “3+2” extension, we consider the following benchmark choice of parameters:

$$m_4 = m_5, \quad s_{14} = s_{15} = 5 \times 10^{-4}, \quad s_{24} = s_{25} = 0.01, \quad s_{34} = s_{35} = 0.1, \quad (51)$$

and further take several choices of mass of the heavy states, which are assumed to be degenerate (i.e. $m_4 = m_5$). For simplicity, we begin by setting all phases to zero; we will subsequently consider their effect for specific observables.

We begin by addressing the scattering cross-sections, studying them for different lepton flavours in the final state, and as a function of the centre-of-mass energy.

Total cross-section Starting from the differential cross-section given in Eq. (3), we can integrate over the scattering angle in the centre-of-mass system to obtain the total cross-section as

$$\sigma_{\text{tot}} = \int_{-1}^{+1} d \cos \theta \frac{d\sigma}{d \cos \theta}. \quad (52)$$

For practical purposes however, one should keep in mind that detectors at a circular collider experiment do not typically exhibit a full “ 4π -coverage”; consequently, one has to impose a cut-off of the integrated angle. However, and instead of imposing a cut on the angle in the laboratory or centre-of-mass frame, we opt to transform the integration variable to pseudo-rapidities via

$$\eta = -\log \left(\tan \left(\frac{\theta}{2} \right) \right), \quad (53)$$

$$d \cos \theta = \frac{1}{\cosh^2 \eta} d\eta. \quad (54)$$

This has the advantage of allowing to impose some physically meaningful cuts on the phase space integration. We adopt here the value of rapidity coverage envisaged for the ATLAS HL-LHC upgrade, which is $|\eta| \leq 4$ [111]. After consistently rewriting the squared amplitude with η rather than $\cos \theta$ and multiplying the cross-section with the Jacobian of Eq. (54), the phase space integration thus becomes

$$\sigma_{\text{tot}} = \int_{\eta_{\text{min}}}^{\eta_{\text{max}}} \frac{1}{\cosh^2 \eta} d\eta \frac{d\sigma}{d\eta}. \quad (55)$$

The results are displayed in Fig. 4, in which we display the cross-sections for different flavour contents of the final state, with respect to \sqrt{s} , for different values of the heavy sterile states. In each panel we also include the proposed μ TRISTAN centre-of-mass energies $\sqrt{s} \in \{126.5, 346.4, 447.2, 1095.4\} \text{ GeV}$ (cf. Table 1). We notice that the benchmark point chosen in Eq. (51) is mostly consistent with low-energy cLFV observables, as will be discussed later in greater detail.

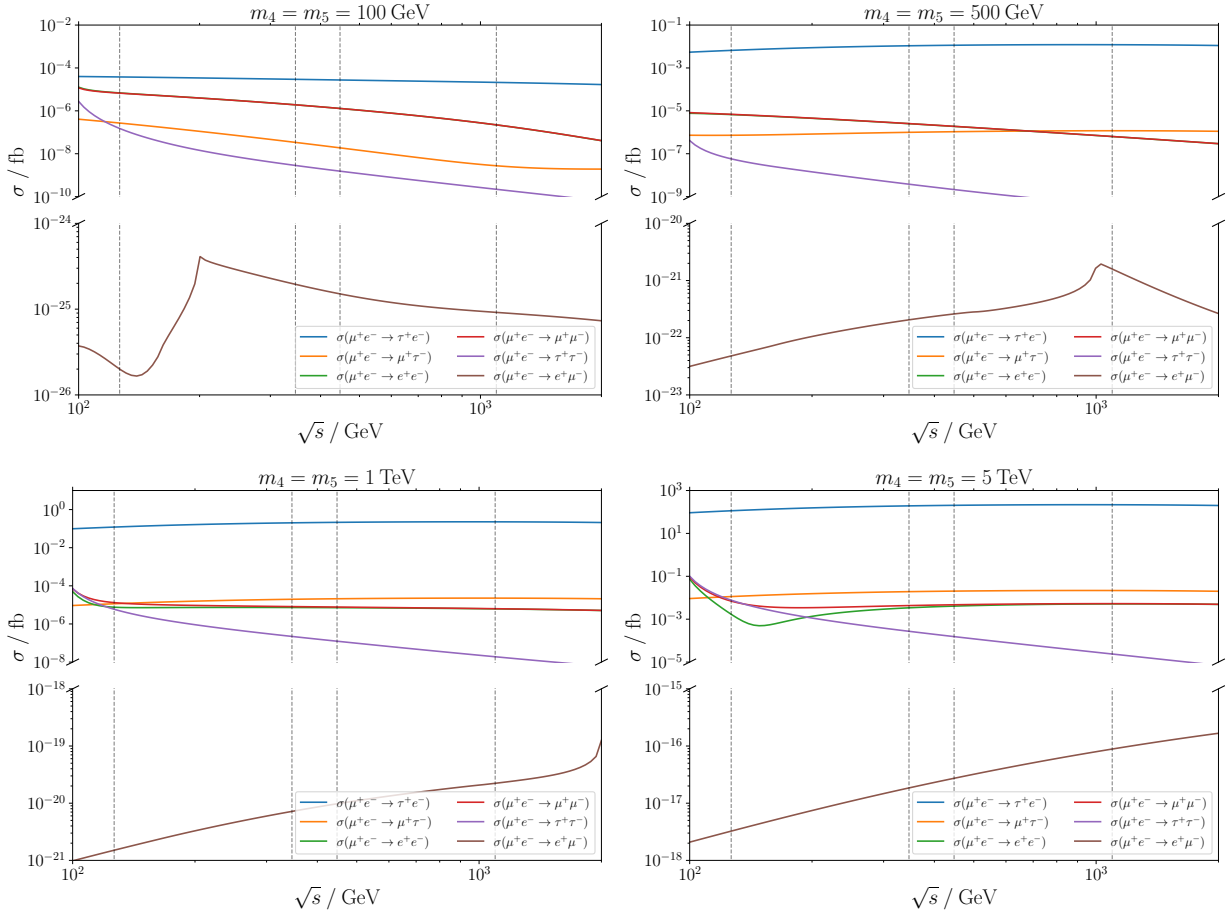


Figure 4: Behaviour of the different cross-sections for $\mu^+e^- \rightarrow \ell_\alpha^+\ell_\beta^-$ with respect to \sqrt{s} . The mixing angles are set as given in Eq. (51), and we show the results for four different choices of HNL masses with $m_4 = m_5 \in \{0.1, 0.5, 1, 5\}$ TeV (from left to right from top to bottom). The dashed vertical lines denote the proposed centre-of-mass energies $\sqrt{s} \in \{126.5, 346.4, 447.2, 1095.4\}$ GeV.

As manifest, processes in association with the t-channel penguins (with either spectator-electron or spectator-muon fermion lines - see the first two diagrams of Fig. 1) exhibit a near independence with respect to \sqrt{s} (only for much larger values of \sqrt{s} , lying outside the range here displayed, would there be a decrease in the -cross-section). For e^+e^- and $\mu^+\mu^-$ final states, there are competing s- and t-channel contributions: for lower regimes of \sqrt{s} , the s-channel contribution dominates (decreasing with \sqrt{s}); for intermediate c.o.m. energies, one can have interference between s- and t-channel contributions; ultimately for larger values of \sqrt{s} , t-channel contributions dominate, leading to an increase in the scattering cross-section. We highlight that this is only fully visible for the case of $m_{4,5} = 5$ TeV. For final states composed of tau pairs, and as can be seen from Fig. 4, s-channel contributions are relevant for the explored regimes (c.o.m. energy and mass scale of the HNLs). Finally, one can verify that box contributions (as those at the source of $\mu^+e^- \rightarrow e^+\mu^-$) are in general subdominant.

A complementary view regarding the behaviour of the cross-section with respect to the mass scale of the heavy spectrum can be found in Figure 5. (Notice that since in this ad-hoc realisation HNL masses are varied while keeping couplings fixed, one trivially recovers the expected increase of the cross-section for increasing masses of the new heavy fermions entering in the corresponding loop-functions.) The small “dip” occurring in the line corresponding to $\mu^+e^- \rightarrow \tau^+\tau^-$ reflects the threshold corresponding to the W^+W^- mediated loop on the associated s-channel penguin contribution.

Pseudo-rapidity distributions and forward-backward asymmetry It is also relevant to consider the prospects of these high-energy CLFV observables regarding angular distributions: in Figure 6 we present an overview of differential distribution with respect to the pseudo-rapidity (normalised to the total cross-section, in order to improve the visibility of the results), setting $m_4 = m_5 = 1$ TeV. As

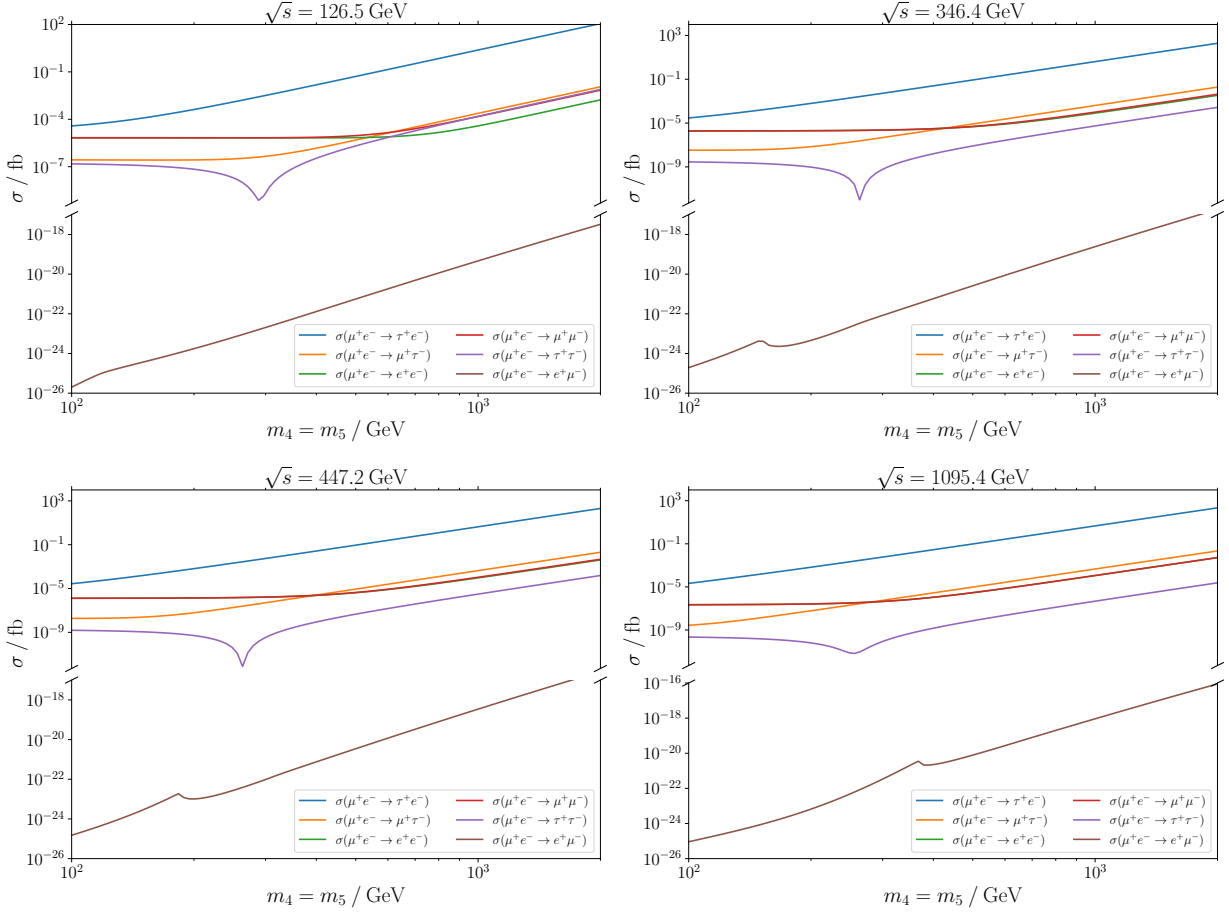


Figure 5: Behaviour of the different cross-sections $\mu^+e^- \rightarrow \ell_\alpha^+\ell_\beta^-$ with respect to $m_4 = m_5$. The mixing angles are set as given in Eq. (51), and we show the results for the four proposed centre-of-mass energies $\sqrt{s} \in \{126.5, 346.4, 447.2, 1095.4\}$ GeV (from left to right from top to bottom).

manifest from all panels, processes exhibiting a strong t-channel penguin dominance are associated to a considerably larger number of events in the forward region, which potentially allows for efficient signal and background discrimination. In particular, this is the case of τ^+e^- , μ^+e^- , e^+e^- and $\mu^+\mu^-$. In Figure 6 one can also see the different interference patterns between s- and t-channel penguins. This is especially true for the $\mu^+e^- \rightarrow e^+e^-$ and $\mu^+e^- \rightarrow \mu^+\mu^-$ scatterings. While the $\mu^+e^- \rightarrow e^+e^-$ distribution displays a cancellation (or rather a “dip”) for most of the considered \sqrt{s} , this feature is absent in the $\mu^+e^- \rightarrow \mu^+\mu^-$, since the t-channel penguin enters differently in the amplitudes of Eq. (2) (see also Eqs. (29-34)). Furthermore, we have considered the forward-backward asymmetry, $A_{FB}(\mu^+e^- \rightarrow \ell_\alpha^+\ell_\beta^-)$. For 2 \rightarrow 2 processes, the forward-backward asymmetry is commonly defined as

$$A_{FB} = \frac{\sigma_F - \sigma_B}{\sigma_F + \sigma_B}, \quad (56)$$

$$\sigma_F = \int_0^{\eta_{\max}} d\eta \frac{d\sigma}{d\eta}, \quad \sigma_B = \int_{\eta_{\min}}^0 d\eta \frac{d\sigma}{d\eta}, \quad (57)$$

in which, as previously stated, we have imposed the cut $|\eta| \leq 4$ for the computation of $\sigma_{F,B}$. We present some numerical results on A_{FB} : first, as a function of the c.o.m energy in Figure 7 (for two fixed values of the heavy fermion masses, 1 TeV and 5 TeV); versus the (degenerate) masses of the HNL (for two of the proposed c.o.m. energies, $\sqrt{s} = 126.5$ GeV and $\sqrt{s} = 346.4$ GeV), as shown in Figure 8. As can be seen, for the two nominal operating \sqrt{s} values, a measurement of the different forward-backward asymmetries could provide complementary information to that solely arising from the total cross-section; as visible from the illustrative examples presented, A_{FB} is clearly sensitive to the topology of the cLFV process, and can help clarifying the underlying nature of the (dominant)

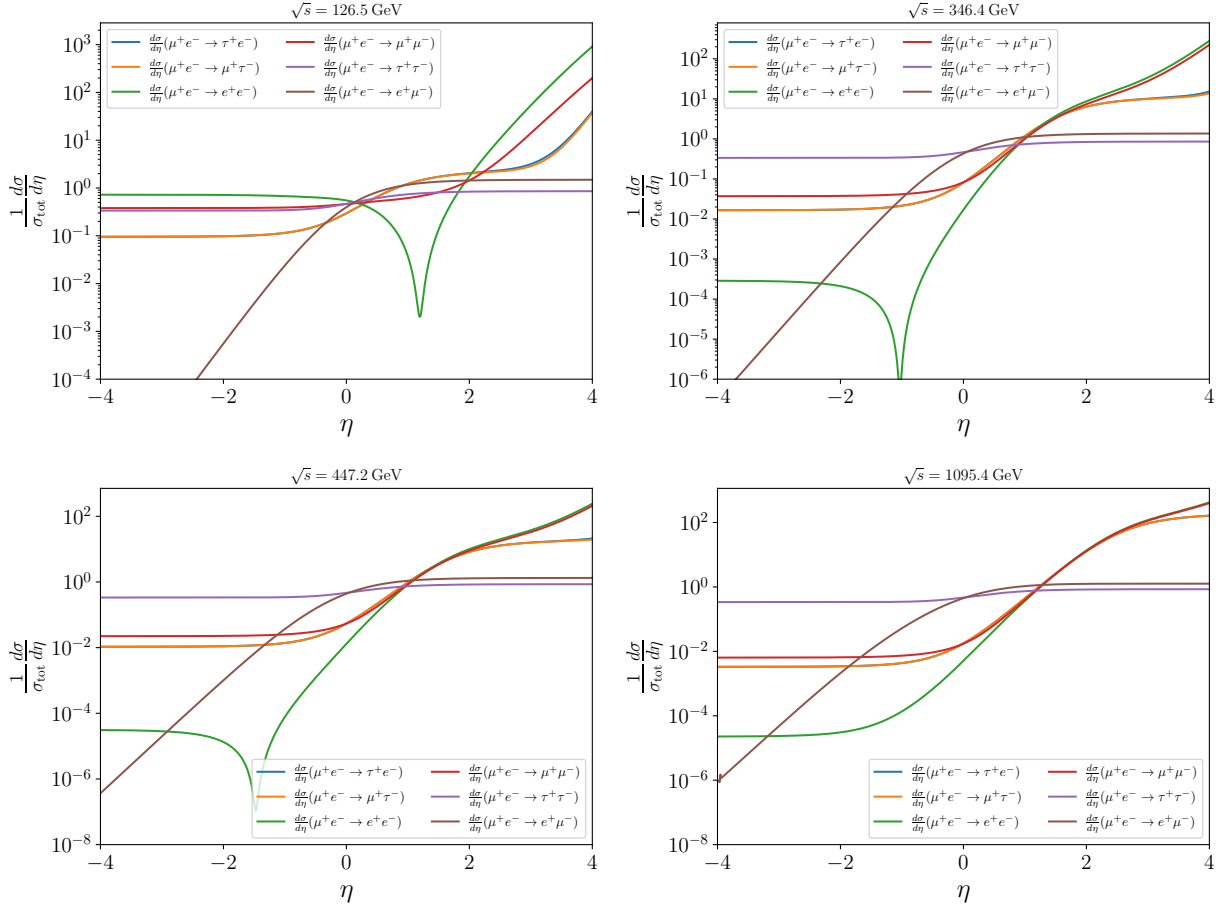


Figure 6: Behaviour of the differential distribution $d\sigma/d\eta$ (normalised to σ_{tot} with respect to the pseudo-rapidity η , for the different processes $\mu^+e^- \rightarrow \ell_\alpha^+\ell_\beta^-$ under discussion. The mixing angles are as given in Eq. (51), and we have set $m_4 = m_5 = 1$ TeV. The panels correspond to the proposed centre-of-mass energies $\sqrt{s} \in \{126.5, 346.4, 447.2, 1095.4\}$ GeV (from left to right from top to bottom).

contribution to the cLFV scatterings. Moreover, a combination of both measurements could hint at the mass-scale of the HNL at the source of the cLFV transitions.

Furthermore, the different A_{FB} are in principle sensitive to new CP-violating phases in the generalised lepton mixing matrix. In order to illustrate this, we have considered the effect of a (Dirac) phase, δ_{24} , and the results are shown in Figure 9. This can be simply understood by considering that the phases lead to a suppression of the Z -penguins (depending on the flavour content of the transitions), such that the interference between the s- and t-channel penguins in $\mu^+e^- \rightarrow e^+e^-$ and $\mu^+e^- \rightarrow \mu^+\mu^-$ will be altered by the presence of non-vanishing CP phases.

Complementary approaches to cLFV: low energies and μ TRISTAN The results so far obtain suggest that μ TRISTAN offers very interesting possibilities to search for cLFV $2 \rightarrow 2$ scatterings, as those induced by the presence of HNL states (and a non-unitary leptonic mixings). The question that must now be addressed is how competitive the μ TRISTAN cLFV searches are when compared to the sensitivity of low-energy searches and those performed at the Z -pole at FCC-ee.

For the illustrative flavour-mixing benchmark here considered (in the context of the minimal ad-hoc extension), it is interesting to notice that μ TRISTAN offers indeed very good prospects to discover HNL through cLFV $\mu^+e^- \rightarrow \ell_\alpha^+\ell_\beta^-$ scatterings. In order to substantiate this, we compare the scattering cross-sections $\mu^+e^- \rightarrow \ell_\alpha^+\ell_\beta^-$ with cLFV processes involving $\mu - \ell_\alpha$ and/or $e - \ell_\beta$ transitions: for example, it is pertinent to compare $\mu^+e^- \rightarrow \tau^+e^-$ with $\tau \rightarrow 3\mu$ and $Z \rightarrow \mu\tau$ decays. This is carried out in Figure 10, whose panels offer a direct comparison of $\sigma(\mu^+e^- \rightarrow \ell_\alpha^+\ell_\beta^-)$ with rare cLFV decays relying on the same flavour violating transitions. Taking $\sqrt{s} = 346.4$ GeV, we compare the scattering

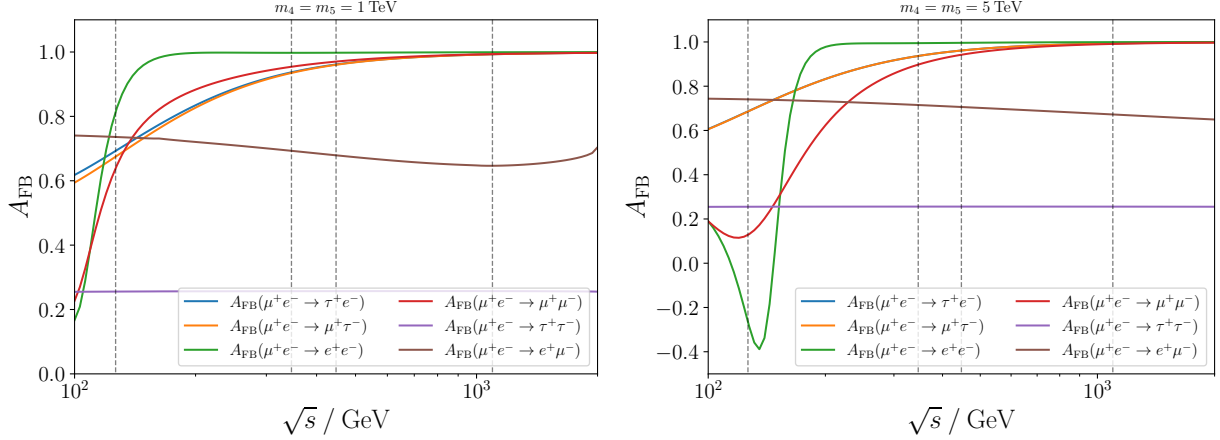


Figure 7: Forward-backward asymmetry with respect to the c.o.m energy for two choices of the HNL masses. The mixing angles are as given in Eq. (51).

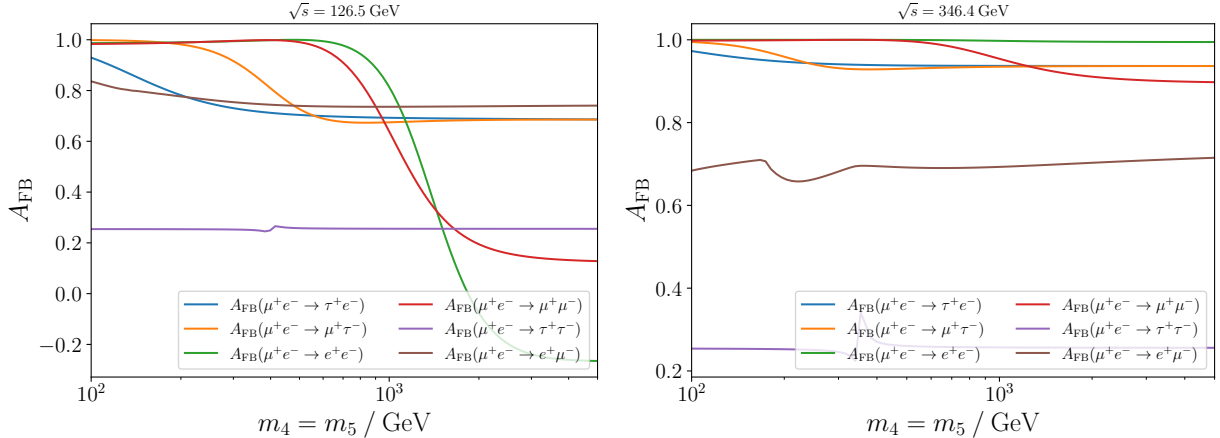


Figure 8: Forward-backward asymmetry with respect to the HNL masses for two choices of the c.o.m energy. The mixing angles are as given in Eq. (51).

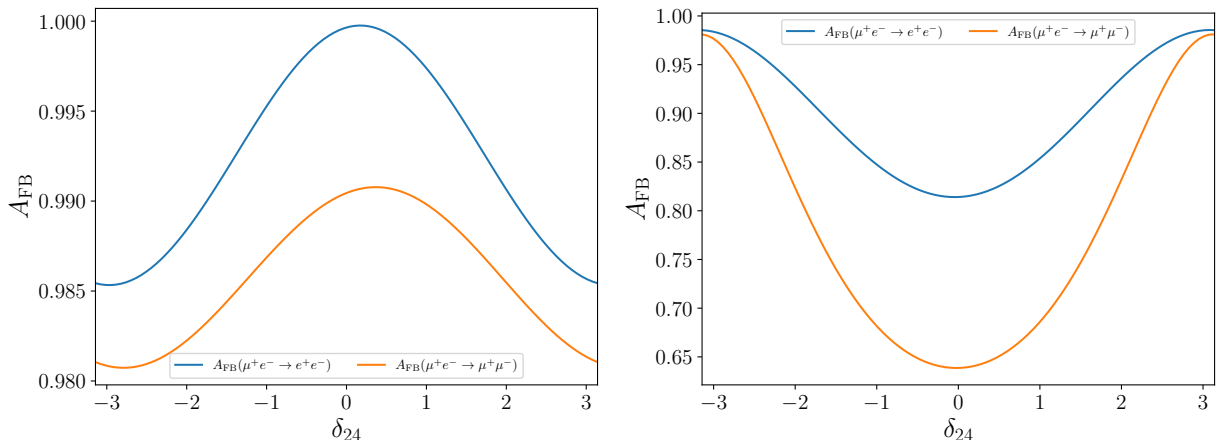


Figure 9: Variation of the forward-backward asymmetries for ee and $\mu\mu$ final states with respect to the CP phase δ_{24} , with the mixing angles as given in Eq. (51). We have set $\sqrt{s} = 126.5$ GeV. On the left, $m_4 = m_5 = 500$ GeV, while on the right $m_4 = m_5 = 1$ TeV.

cross-sections with the relevant branching ratios for varying values of the heavy sterile states.

The comparison of $\sigma(\mu^+e^- \rightarrow \tau^+e^-)$ with the prospects for leptonic cLFV tau decays and $Z \rightarrow \ell\tau$ decays (displayed in the top-left panel of Fig. 10) clearly shows that, for the “3+2” flavour benchmark under consideration, one can expect tens (or even hundreds) of thousands of events at μ TRISTAN⁵. This clearly highlights how such an asymmetric lepton collider can be competitive or even out-perform the prospects for observing cLFV decays involving tau leptons.

It is also interesting to comment on a cLFV low-energy observable that strongly resembles $\mu^+e^- \rightarrow e^+\mu^-$ scattering: muonium oscillations. As can be seen from the lower right-hand panel of Fig. 10, both the scattering processes at μ TRISTAN, and the oscillation probability clearly lie beyond any prospect for observation.

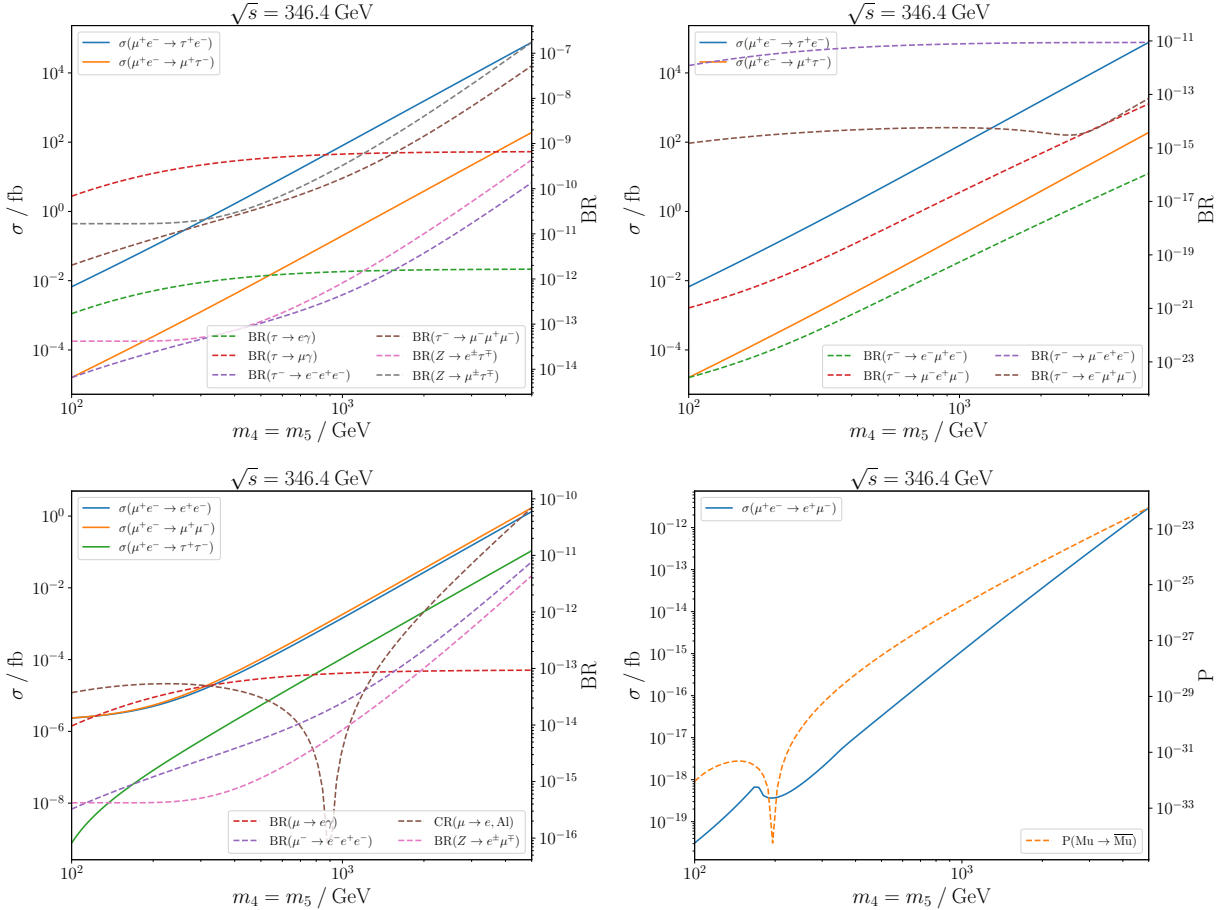


Figure 10: Comparative prospects for cLFV processes: $\sigma(\mu^+e^- \rightarrow \ell_\alpha^+\ell_\beta^-)$ as a function of the (degenerate) HNL masses for $\sqrt{s} = 346.4$ GeV. On the secondary y -axes (right hand-side of each plot) we display the rates for associated cLFV processes: radiative and 3-body decays, neutrinoless muon-conversion in matter, muonium oscillations and cLFV Z boson decays.

We emphasise here the comparative study presented in Figure 10 should not be perceived as a generic feature of these minimal ad-hoc extensions. Nevertheless, it can be interpreted as a strong *proof of merit* that μ TRISTAN offers rich prospects for the observation of cLFV - even in the absence of other signals (Z decays and/or low-energy transitions).

5.2 ISS(3,3)

After a first approach to the cLFV observables that can be studied at μ TRISTAN, relying on the simple minimal SM extension via 2 HNL, we now proceed to consider a complete model of neutrino mass generation. Contrary to the ad-hoc model, we recall that in such a case NP mass scales and

⁵Relying on a conservative estimate of the efficiency, $\mathcal{O}(1\%)$, and for the nominal luminosities, see Section 2.

couplings are intrinsically connected by the need to accommodate neutrino oscillation data. It is nevertheless important to notice that the behaviours discussed above for the ad-hoc minimal extension are representative of generic SM extensions via HNLs; the (relative) weights of the cLFV form-factors naturally reflect the actual model under consideration, but the qualitative features are expected to hold for the case of a complete model as the (3,3) realisation of the ISS (described in Section 4).

In particular, the goal of this final study is to highlight through a complete NP model the complementary role that μ TRISTAN can play in the landscape of cLFV searches.

In order to illustrate our findings in a concrete and efficient manner, we rely on the modified Casas-Ibarra parametrisation (see Eq. (44)) to determine the Yukawa couplings while in agreement with oscillation data. We set the orthogonal Casas-Ibarra R -matrix to unity and assume a diagonal and universal $\mu_X = 10^{-6}$ GeV (at this first stage); we further assume M_R to be diagonal and universal. Concerning the active neutrino parameters, the PMNS entries have been set to the central values according to NuFit6.0 [71], and the lightest neutrino mass to $m_0 = 10^{-5}$ eV (we only consider normal ordering (NO)). The benchmark “flavour-space” thus obtained - since M_R is not fixed - reflects an ensemble of realistic cases which have not yet been excluded by current bounds on cLFV processes nor from leading to large deviations from unitarity of the would-be PMNS.

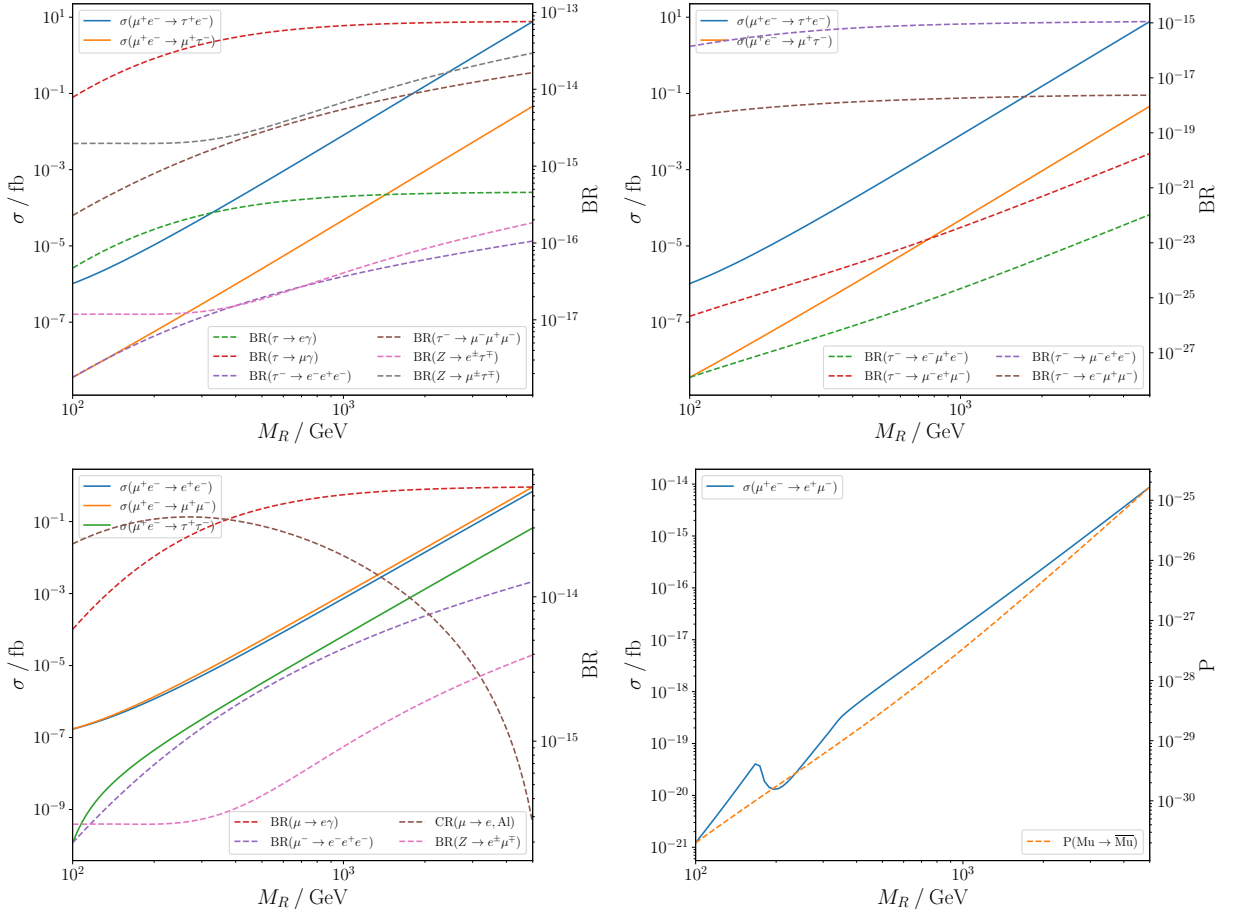


Figure 11: Comparative prospects for cLFV processes: $\sigma(\mu^+e^- \rightarrow \ell_\alpha^+\ell_\beta^-)$ as a function of the (degenerate) M_R masses, for $\mu_X = 10^{-6}$ GeV and $\sqrt{s} = 346.4$ GeV. On the secondary y -axes (right side of each plot) we display the rates for associated cLFV processes: radiative and 3-body decays, neutrinoless muon-conversion in matter, muonium oscillations and cLFV Z boson decays.

To begin our discussion, we reproduce in Figure 11 an analogous study to that of Figure 10 (for the ad-hoc model), comparing $\sigma(\mu^+e^- \rightarrow \ell_\alpha^+\ell_\beta^-)$ with several cLFV branching rates, as a function of the (degenerate) M_R masses. As can be seen, the cLFV rates for processes involving τ -leptons at low energies and in Z -decays all lie below any future sensitivities, while the cross-sections for $\mu^+e^- \rightarrow \tau^+e^-$ and $\mu^+e^- \rightarrow \mu^+\tau^-$ scattering can reach sizeable values, leading to hundreds or even

thousands of events that could be potentially observed by μ TRISTAN. For $\mu - e$ violating processes, searches at μ TRISTAN cannot compete with low-energy probes, in agreement with the expectations arising from the study of the ad-hoc model of the previous subsection.

In view of the sizeable cross-sections, it is worthwhile to carry out a naïve analysis of the potential of the μ TRISTAN collider in constraining the parameter space of the ISS(3,3). Still relying on the Casas-Ibarra parametrisation - as described before - we nevertheless depart from the simple hypothesis of fixed μ_X , and explore the ISS(3,3) space spanned by the NP scale M_R and the size of the LNV parameter, μ_X .

In the absence of concrete detector designs, a full study of possible backgrounds and systematics is clearly beyond the scope of this work. However, we can make some preliminary estimates and identify sources of the latter. Firstly, a foreseeable improvement from the theory side is the inclusion of QED corrections (virtual and real) which will affect not only the overall cross-sections but also the event shapes. A proper computation of the $2 \rightarrow 3$ scattering cross-sections (with an additional photon from initial state or final state radiation) would also allow scanning over “effective” \sqrt{s} c.o.m. energies (making use of the so-called radiative return), similarly to what was done at LEP.

Experimentally, and if we assume the PMNS paradigm, one can envisage backgrounds from $\mu^+ e^- \rightarrow \ell_\alpha^+ \ell_\beta^- \nu \nu$ production. As an example, we estimate the total cross-section of $\mu^+ e^- \rightarrow \tau^+ e^- \nu \nu$ background to be (at leading order) $\sigma_{\text{bkg}} \simeq 21 \text{ fb}$. This can be significantly reduced by imposing very basic cuts by selecting events with small (or vanishing) missing energy $\cancel{E}_T \leq 10 \text{ GeV}$ and events that mostly lie in the forward region (see Figure 6). By further demanding $2.0 \leq \eta_\ell \leq 4.0$, we reduce the background cross-section to $\sigma_{\text{bkg, cut}} \simeq 6 \times 10^{-4} \text{ fb}$, so that for an integrated luminosity of 1 ab^{-1} less than one background event is expected. The signal efficiency for these very basic cuts is 25%; combined with a conservatively estimated τ -tagging efficiency of 40% [112] we can estimate the total signal efficiency at $\simeq 10\%$. Allowing for further signal loss due to charge and particle misidentification, as well as beam contamination due to in-flight decaying muons, we take a total signal efficiency of 1% as a conservative estimate (while reducing the backgrounds to negligible levels). We demand a detection of (at least) 10 signal events with negligible backgrounds for our sensitivity estimates, leading to a total significance of

$$\mathcal{S} = \frac{S}{\sqrt{S + B}} \sim 3\sigma. \quad (58)$$

Our results are shown in Figure 12 for $\mu - e$ flavour violation (on the left) and for processes involving τ -leptons (on the right). We draw sensitivity contours in the $(M_R - \mu_X)$ plane for current bounds on low-energy cLFV processes (see legends) and future sensitivities of dedicated facilities (cf. Table 2), the latter corresponding to a darker-to-lighter shading. Onto this we superimpose the sensitivities of a μ TRISTAN collider obtained with the previously outlined analysis, assuming 100 fb^{-1} (solid lines) and 1 ab^{-1} (dashed lines) luminosities.

As can be seen, for $\mu - e$ sector flavour violation, searches at μ TRISTAN cannot compete with low-energy processes at dedicated high-intensity facilities - MEG II, Mu3e, as well as COMET and Mu2e. For flavour violating processes involving τ -leptons, the situation is however much more promising, as searches at μ TRISTAN vastly outperform future bounds on cLFV τ -lepton decays, leading to a sensitivity reach that is several orders of magnitude larger.

Interestingly, μ TRISTAN is also very competitive with cLFV Z -boson decays - even in view of the most optimistic expectations of a future Tera- Z factory. The contours for cLFV Z -boson decays, together with μ TRISTAN searches for $\mu^+ e^- \rightarrow \tau^+ e^-$ and $\mu^+ e^- \rightarrow \mu^+ \tau^-$ scatterings are shown in Figure 13, for 100 fb^{-1} and 1 ab^{-1} luminosities. As can be seen, the expected sensitivities of a future Tera- Z factory are vastly outperformed by dedicated searches at μ TRISTAN, highlighting the strong complementarity role of such a collider. This is further reinforced by recalling that searches at the Z -pole are in general plagued by irreducible systematics.

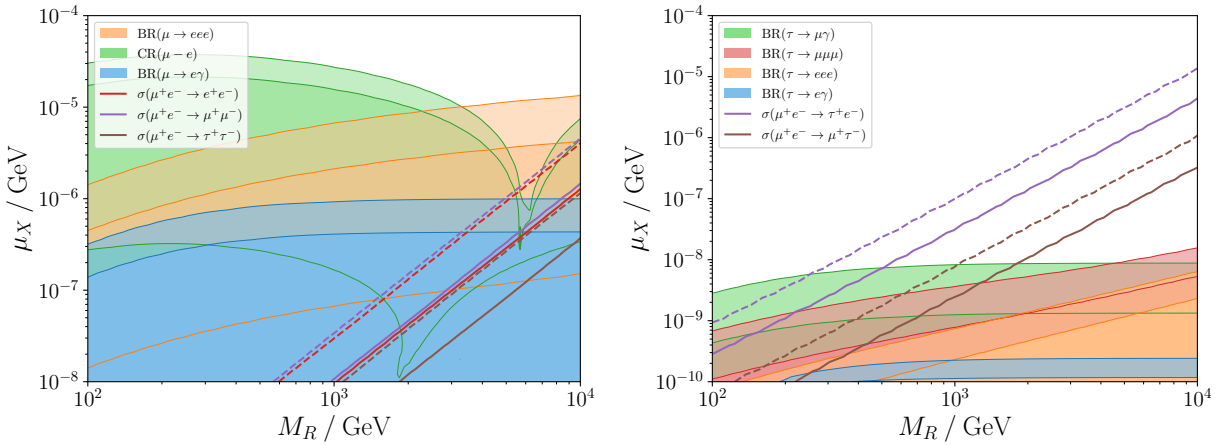


Figure 12: Prospects for ISS(3,3) cLFV searches depicted in the $(M_R - \mu_X)$ plane: for bounds on low-energy cLFV processes, darkest to lightest shading correspond to current bounds and (distinct) future sensitivities, see Table 2. (Notice that for $\mu - e$ conversion there are distinct shadings for the two future Mu2e and COMET sensitivities; likewise, the Mu3e phase 1 and phase 2 correspond to different shades.) Expected μ TRISTAN cross-sections for 1% efficiency and 100 fb^{-1} luminosity (1 ab^{-1}) are given by solid (dashed) lines.

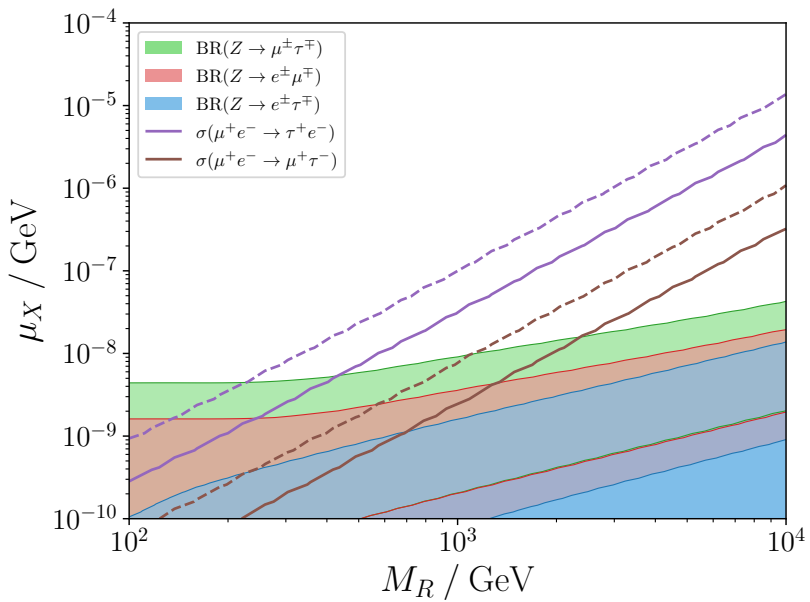


Figure 13: Prospects for ISS(3,3) cLFV searches depicted in the $(M_R - \mu_X)$ plane: current and future bounds of cLFV Z decays (shaded regions, cf. Table 2) together with the projected sensitivity of μ TRISTAN searches for $\mu^+ e^- \rightarrow \tau^+ e^-$ and $\mu^+ e^- \rightarrow \mu^+ \tau^-$ scatterings. For the cross-sections, solid (dashed) lines correspond to 100 fb^{-1} luminosity (1 ab^{-1}).

6 Concluding remarks and outlook

In this work we have addressed the sensitivity of an asymmetric lepton collider to cLFV signals, as those originating from the presence of heavy sterile states. Focusing on μ TRISTAN [50], we have thus explored the prospects for observing cLFV lepton scatterings $\mu^+ e^- \rightarrow \ell_\alpha^+ \ell_\beta^-$, studying two phenomenological frameworks: a minimal ad-hoc SM extension via two heavy neutral leptons, and a simple realisation of the Inverse Seesaw, the ISS(3,3).

We have carried out a full, detailed computation of the cross-sections for $\mu^+ e^- \rightarrow \ell_\alpha^+ \ell_\beta^-$ scattering, as well as other observables, such as rapidity distributions and forward-backward asymmetries. The asymmetries have been shown to offer valuable help in distinguishing the nature of dominant contributions - for instance loop- versus tree-level exchanges, and in the latter case provide important information on the mass of the mediators [55]. The full expressions for the observables are given in detail, and in a user-friendly way.

As a first approach to illustrate the potential of μ TRISTAN cLFV searches, we have considered a flavour-benchmark configuration for a minimal, ad-hoc SM extension via 2 HNLs (encoding their role in an enlarged leptonic mixing matrix). Such a first, simple approach nevertheless clearly reveals that the reach of μ TRISTAN might offer interesting, and clearly complementary probes in the search for cLFV at high-energies. Possible measurements of the rapidity distributions and A_{FB} are further complementary and might offer valuable insight onto the underlying topology of the exchanges. Furthermore, we have pointed out that such observables might also be sensitive to new sources of CP violation in the lepton sector.

These effects could be further explored with the possibility of beam polarisation (expected to be $\mathcal{O}(90\%)$ for μ^+ and $\mathcal{O}(70\%)$ for e^-), which would allow to better identify the nature of the NP mediators. Let us mention that here we have only considered fully leptonic processes - one could envisage addressing $\mu^+ e^- \rightarrow q\bar{q}$ production, as this would allow exploring possible connections to the most constraining low-energy cLFV transition (i.e. $\mu - e$ conversion, in view of the impressive future sensitivities), and possibly to leptonic meson decays.

We have then considered a well-motivated model of neutrino mass generation, which constitutes a complete realisation featuring the essential building blocks present in the SM ad-hoc extension. Our study of the ISS supports our assessment of the role of μ TRISTAN: not only is it complementary to low-energy cLFV searches, but it also offers much stronger probes for cLFV involving τ -leptons (being remarkably sensitive to Z -penguin exchanges, even more than leptonic cLFV decays or cLFV Z decays). Although we have not considered it here, one expects that such a probing power is also manifest for other low-energy seesaw realisation, as for instance the Linear Seesaw.

For $\tau - \ell$ flavour violation, μ TRISTAN offers rich prospects for the observation of cLFV processes - even in the absence of other signals (Z decays and/or low-energy transitions). Strikingly, even for 5×10^{12} Z bosons, due to an irreducible systematic misidentification of secondary leptons from the τ decays in $Z \rightarrow \tau\tau$ as primary leptons in $Z \rightarrow \ell\tau$, μ TRISTAN is clearly more sensitive to $\mu - \tau$ flavour violation (via Z -penguin exchange) than FCC-ee.

Acknowledgements

JK is supported by the Slovenian Research Agency under the research grant No. N1-0253 and in part by J1-3013. JK is grateful for the hospitality of the Theory group of the Laboratoire de physique de Clermont Auvergne where large parts of this work have been completed and JK is further grateful to Miha Nemevšek for useful suggestions. EP acknowledges financial support from the Swiss National Science Foundation (SNF) under contract 200020 204428. This project has received support from the European Union's Horizon 2020 research and innovation programme under the Marie Skłodowska-Curie grant agreement No. 860881 (HIDDe ν network) and from the IN2P3 (CNRS) Master Project, "Hunting for Heavy Neutral Leptons" (12-PH-0100).

A Feynman rules for relevant vertices

The extended lepton sector will lead to modified charged and neutral current interactions. For the case of Majorana neutral fermions, the most relevant terms (for the purpose of the current study) are collected below. In particular, we include interactions with neutral and charged gauge bosons, Higgs and Goldstone bosons.

$$\begin{aligned}
\mathcal{L}_{W^\pm} &= -\frac{g_w}{\sqrt{2}} W_\mu^\pm \sum_{\alpha=1}^3 \sum_{j=1}^{3+n_S} \mathcal{U}_{\alpha j} \bar{\ell}_\alpha \gamma^\mu P_L \nu_j + \text{H.c.}, \\
\mathcal{L}_{Z^0} &= -\frac{g_w}{4 \cos \theta_w} Z_\mu \sum_{i,j=1}^{3+n_S} \bar{\nu}_i \gamma^\mu (P_L \mathcal{C}_{ij} - P_R \mathcal{C}_{ij}^*) \nu_j, \\
\mathcal{L}_{H^0} &= -\frac{g_w}{4 M_W} H \sum_{i \neq j=1}^{3+n_S} \bar{\nu}_i [\mathcal{C}_{ij} (P_L m_i + P_R m_j) + \mathcal{C}_{ij}^* (P_R m_i + P_L m_j)] \nu_j, \\
\mathcal{L}_{G^0} &= \frac{i g_w}{4 M_W} G^0 \sum_{i,j=1}^{3+n_S} \bar{\nu}_i [\mathcal{C}_{ij} (P_R m_j - P_L m_i) + \mathcal{C}_{ij}^* (P_R m_i - P_L m_j)] \nu_j, \\
\mathcal{L}_{G^\pm} &= -\frac{g_w}{\sqrt{2} M_W} G^\pm \sum_{\alpha=1}^3 \sum_{j=1}^{3+n_S} \mathcal{U}_{\alpha j} \bar{\ell}_\alpha (m_\alpha P_L - m_j P_R) \nu_j + \text{H.c.}
\end{aligned} \tag{59}$$

We notice that the above interactions were cast in the physical lepton bases, with Greek indices denoting the flavour of the charged leptons, and $i, j = 1 \dots n_S$ the neutral fermion spectrum (with n_S denoting the number of sterile states). Moreover, \mathcal{C}_{ij} are defined as

$$\mathcal{C}_{ij} = \sum_{\rho=1}^3 \mathcal{U}_{i\rho}^\dagger \mathcal{U}_{\rho j}. \tag{60}$$

In what follows, and for completeness, we present the Feynman rules for the vertices which are used throughout our computation; these correspond to the modified Lagrangian terms which were given in Eq. (59).

Notice that for the case of the Z and Higgs vertices, the arrows denote the momentum flow. Since all physical neutral leptons are assumed to be of Majorana nature, diagrams including at least one $Z n_i n_j$ or $H n_i n_j$ vertex must thus be symmetrised (factor 2). In the case of the W interactions, the curved arrow represents an arbitrary (fermion) flow, see [67] for more details.

B Computation of box-diagram contributions: comments and detailed discussion

While the computation of the penguin diagrams can be performed in Feynman 't-Hooft gauge in a fairly straightforward manner, the box diagrams require significantly more effort and attention. First of all we notice that diagrams (3) and (4) of Figure 3 contain LNV interactions and thus one needs to use the fermion-number violating Feynman rules of [67], which we summarised in Table 3 of Appendix A. This leads, prior to integration, to the following amplitudes:

$$\begin{aligned}
\mathcal{M}_1^{\alpha\beta} &= \int \frac{d^D k}{(2\pi)^D} \bar{v}_\mu(p_1) \left[\left(\frac{-ig}{\sqrt{2}} \right) \mathcal{U}_{\mu i} \gamma_\alpha P_L i \frac{(\not{k} + m_i)}{k^2 - m_i^2} \left(\frac{-ig}{\sqrt{2}} \right) \mathcal{U}_{ei} \gamma_\mu P_L \right] u_e(p_2) \\
&\quad \times \bar{u}_\beta(p_4) \left[\left(\frac{-ig}{\sqrt{2}} \right) \mathcal{U}_{\beta j}^* \gamma_\nu P_L i \frac{(\not{k} + \not{p}_1 - \not{p}_3 + m_j)}{(k + p_1 - p_3)^2 - m_j^2} \left(\frac{-ig}{\sqrt{2}} \right) \mathcal{U}_{\alpha j}^* \gamma_\beta P_L \right] v_\alpha(p_3) \\
&\quad \times \frac{(-ig^{\alpha\beta})}{(k + p_1)^2 - m_W^2} \frac{(-ig^{\mu\nu})}{(k - p_2)^2 - m_W^2},
\end{aligned} \tag{61}$$

$$Z_\mu \sim \text{wavy line} \quad \begin{array}{c} n_i \\ \swarrow \quad \searrow \\ n_j \end{array} = -i \frac{g_w}{4c_w} \gamma_\mu \left(C_{ij}^* P_L - C_{ij} P_R \right)$$

$$H \sim \text{dashed line} \quad \begin{array}{c} n_i \\ \swarrow \quad \searrow \\ n_j \end{array} = -i \frac{g_w}{4M_W} \left[C_{ij} (m_i P_L + m_j P_R) + C_{ij}^* (m_i P_R + m_j P_L) \right]$$

$$W_\mu^- \sim \text{wavy line} \quad \begin{array}{c} \nu_i \\ \swarrow \quad \searrow \\ \ell^- \end{array} = -i \frac{g_w}{\sqrt{2}} \mathcal{U}_{\ell\nu} \gamma_\mu P_L$$

$$W_\mu^+ \sim \text{wavy line} \quad \begin{array}{c} \ell^+ \\ \swarrow \quad \searrow \\ \nu_i \end{array} = -i \frac{g_w}{\sqrt{2}} \mathcal{U}_{\ell\nu}^* \gamma_\mu P_L$$

$$G^- \sim \text{dashed line} \quad \begin{array}{c} \nu_i \\ \swarrow \quad \searrow \\ \ell^- \end{array} = i \frac{g_w}{\sqrt{2}M_W} \mathcal{U}_{\ell\nu} (m_\nu P_R - m_\ell P_L)$$

$$G^+ \sim \text{dashed line} \quad \begin{array}{c} \ell^+ \\ \swarrow \quad \searrow \\ \nu_i \end{array} = i \frac{g_w}{\sqrt{2}M_W} \mathcal{U}_{\ell\nu}^* (m_\nu P_L - m_\ell P_R)$$

$$W_\mu^- \sim \text{wavy line} \quad \begin{array}{c} \ell^- \\ \swarrow \quad \searrow \\ \nu_i \end{array} = -i \frac{g_w}{\sqrt{2}} \mathcal{U}_{\ell\nu} \gamma_\mu (-\mathbf{P}_R)$$

$$W_\mu^+ \sim \text{wavy line} \quad \begin{array}{c} \nu_i \\ \swarrow \quad \searrow \\ \ell^+ \end{array} = -i \frac{g_w}{\sqrt{2}} \mathcal{U}_{\ell\nu}^* \gamma_\mu (-\mathbf{P}_R)$$

$$G^- \sim \text{dashed line} \quad \begin{array}{c} \ell^- \\ \swarrow \quad \searrow \\ \nu_i \end{array} = i \frac{g_w}{\sqrt{2}M_W} \mathcal{U}_{\ell\nu} (m_\nu P_R - m_\ell P_L)$$

$$G^+ \sim \text{dashed line} \quad \begin{array}{c} \nu_i \\ \swarrow \quad \searrow \\ \ell^+ \end{array} = i \frac{g_w}{\sqrt{2}M_W} \mathcal{U}_{\ell\nu}^* (m_\nu P_L - m_\ell P_R)$$

Table 3: Feynman rules for W , Z and Higgs interactions, together with Goldstone bosons in generic SM extensions via Majorana sterile fermions (such as the ad-hoc “3+2” extension, or the ISS(3,3) here considered).

$$\begin{aligned}
\mathcal{M}_2^{\alpha\beta} &= \int \frac{d^D k}{(2\pi)^D} \bar{v}_\mu(p_1) \left[\left(\frac{-ig}{\sqrt{2}} \right) \mathcal{U}_{\mu i} \gamma_\alpha P_L i \frac{(\not{k} - \not{p}_1 + m_i)}{(k - p_1)^2 - m_i^2} \left(\frac{-ig}{\sqrt{2}} \right) \mathcal{U}_{\alpha i}^* \gamma_\mu P_L \right] v_\alpha(p_3) \\
&\quad \times \bar{u}_\beta(p_4) \left[\left(\frac{-ig}{\sqrt{2}} \right) \mathcal{U}_{\beta j} \gamma_\nu P_L i \frac{(\not{k} + \not{p}_2 + m_j)}{(k + p_2)^2 - m_j^2} \left(\frac{-ig}{\sqrt{2}} \right) \mathcal{U}_{\beta j}^* \gamma_\nu P_L \right] u_e(p_2) \\
&\quad \times \frac{(-ig^{\alpha\beta})}{k^2 - m_W^2} \frac{(-ig^{\mu\nu})}{(k - p_1 + p_3)^2 - m_W^2}, \tag{62}
\end{aligned}$$

$$\begin{aligned}
\mathcal{M}_3^{\alpha\beta} &= \int \frac{d^D k}{(2\pi)^D} \bar{v}_\mu(p_1) \left[\left(\frac{-ig}{\sqrt{2}} \right) \mathcal{U}_{\mu i} \gamma_\alpha P_L i \frac{(\not{k} - \not{p}_1 + m_i)}{(k - p_1)^2 - m_i^2} \left(\frac{-ig}{\sqrt{2}} \right) \mathcal{U}_{\beta i} \gamma_\mu (-P_R) \right] \mathbf{v}_\beta(p_4) \\
&\quad \times \bar{u}_\alpha(p_3) \left[\left(\frac{-ig}{\sqrt{2}} \right) \mathcal{U}_{\alpha j}^* \gamma_\nu (-P_R) i \frac{(\not{k} + \not{p}_2 + m_j)}{(k + p_2)^2 - m_j^2} \left(\frac{-ig}{\sqrt{2}} \right) \mathcal{U}_{\alpha j}^* \gamma_\nu P_L \right] u_e(p_2) \\
&\quad \times \frac{(-ig^{\alpha\beta})}{k^2 - m_W^2} \frac{(-ig^{\mu\nu})}{(k + p_2 - p_3)^2 - m_W^2}, \tag{63}
\end{aligned}$$

$$\begin{aligned}
\mathcal{M}_4^{\alpha\beta} &= \int \frac{d^D k}{(2\pi)^D} \bar{v}_\mu(p_1) \left[\left(\frac{-ig}{\sqrt{2}} \right) \mathcal{U}_{\mu i} \gamma_\alpha P_L i \frac{(\not{k} - \not{p}_1 + \not{p}_3 + m_i)}{(k - p_1 + p_3)^2 - m_i^2} \left(\frac{-ig}{\sqrt{2}} \right) \mathcal{U}_{\beta i} \gamma_\mu (-P_R) \right] \mathbf{v}_\beta(p_4) \\
&\quad \times \bar{u}_\alpha(p_3) \left[\left(\frac{-ig}{\sqrt{2}} \right) \mathcal{U}_{\alpha j}^* \gamma_\beta (-P_R) i \frac{(-\not{k} + m_j)}{k^2 - m_j^2} \left(\frac{-ig}{\sqrt{2}} \right) \mathcal{U}_{\alpha j}^* \gamma_\nu P_L \right] u_e(p_2) \\
&\quad \times \frac{(-ig^{\alpha\beta})}{(k + p_3)^2 - m_W^2} \frac{(-ig^{\mu\nu})}{(k + p_2)^2 - m_W^2}, \tag{64}
\end{aligned}$$

in which we colour-highlight the flip $P_L \rightarrow -P_R$ in the fermion-number violating W -vertices (cf. Appendix A) as well as the spinor-flip $u \leftrightarrow v$ (see [67] for details). Moreover, one has to add the corresponding Goldstone diagrams to obtain physical amplitudes; we stress here that the corresponding Goldstone vertices do not feature the $P_L \leftrightarrow -P_R$ flip as shown in Table 3.

After extensive algebraic transformations (or after using software like **package-X** [113] or **FeynCalc** [114–116] as done here), one encounters “unusual” Dirac structures in the integrated and simplified amplitudes (in $D = 4 - 2\epsilon$ dimensions), which can be reduced to the chiral Dirac basis with the help of the identities derived in Appendix C. Here, we just summarise the results which we obtain in the limit of massless external fermions.

The amplitudes of box-diagrams (1) and (2) admit, in addition to $[\bar{v}\gamma_\mu P_L v][\bar{u}\gamma^\mu P_L u]$, the following “unusual” Dirac structures (with the short-hand notation: $u_i/v_i \equiv u/v(p_i)$)

$$[\bar{v}_1 p_3 P_L u_2][\bar{u}_4 p_2 P_L v_3] = -[\bar{v}_1 p_3 P_L u_2][\bar{u}_4 p_1 P_L v_3], \tag{65}$$

and

$$[\bar{v}_1 p_2 P_L v_3][\bar{u}_4 p_3 P_L u_2] = -[\bar{v}_1 p_2 P_L v_3][\bar{u}_4 p_1 P_L u_2], \tag{66}$$

in which we used on-shell conditions and the masslessness of the external fermions. Since the box amplitudes are all finite, we can safely take the limit of $\epsilon \rightarrow 0$, that is taking the limit of $D = 4$ spacetime dimensions.

Thus, setting external fermions to be massless and taking the limit $D = 4$, the above Dirac structures can further be reduced to

$$[\bar{v}_1 p_3 P_L u_2][\bar{u}_4 p_1 P_L v_3] = g_{\alpha\beta} p_1^\alpha p_3^\beta [\bar{v}_1 \gamma_\mu P_L u_2][\bar{u}_4 \gamma^\mu P_L v_3], \tag{67}$$

$$[\bar{v}_1 p_2 P_L v_3][\bar{u}_4 p_1 P_L u_2] = g_{\alpha\beta} p_1^\alpha p_2^\beta [\bar{v}_1 \gamma_\mu P_L v_3][\bar{u}_4 \gamma^\mu P_L u_2]. \tag{68}$$

The remaining diagrams admit a plethora of further Dirac structures which can be reduced to a scalar combination multiplied by a scalar product of momenta. These are given by

$$[\bar{v}_1 \sigma_{\mu\alpha} P_R v_4][\bar{u}_3 \sigma^{\mu\beta} P_L u_2] p_3^\alpha p_1^\beta = -g_{\alpha\beta} p_3^\alpha p_1^\beta S_{RL}, \tag{69}$$

$$[\bar{v}_1 \sigma_{\mu\alpha} P_R v_4][\bar{u}_3 \sigma^{\mu\beta} P_L u_2] p_2^\alpha p_1^\beta = g_{\alpha\beta} p_2^\alpha p_1^\beta S_{RL}, \tag{70}$$

$$[\bar{v}_1 \sigma_{\mu\alpha} P_R v_4] [\bar{u}_3 \sigma^{\mu\beta} P_L u_2] p_4^\alpha p_{1\beta} = g_{\alpha\beta} (p_2^\alpha + p_3^\alpha) p_1^\beta S_{RL}, \quad (71)$$

$$[\bar{v}_1 \sigma_{\alpha\beta} P_R v_4] [\bar{u}_3 P_L u_2] p_2^\alpha p_3^\beta = i g_{\alpha\beta} (p_1^\alpha + p_4^\alpha) p_1^\beta S_{RL}, \quad (72)$$

$$[\bar{v}_1 \sigma_{\alpha\beta} P_R v_4] [\bar{u}_3 P_L u_2] p_3^\alpha p_3^\beta = -i g_{\alpha\beta} p_1^\alpha p_3^\beta S_{RL}, \quad (73)$$

$$[\bar{v}_1 \sigma_{\alpha\beta} P_R v_4] [\bar{u}_3 P_L u_2] p_1^\alpha p_2^\beta = -i g_{\alpha\beta} p_1^\alpha p_2^\beta S_{RL}, \quad (74)$$

with $\sigma^{\mu\nu} = \frac{i}{2} [\gamma^\mu, \gamma^\nu]$ and brackets denote the commutator. We have also introduced the abbreviation

$$S_{RL} = [\bar{v}_1 P_R v_4] [\bar{u}_3 P_L u_2]. \quad (75)$$

We stress again that these identities are only valid in the limit of massless external fermions ⁶. The derivation of most of these identities require several non-trivial steps, which we outline in the following appendix.

C Notes on Diracology

In the interest of reproducibility, and for the reader's convenience, we outline the main steps necessary to find the identities given in Eqs. (67-74). First of all, let us note, since we work exclusively in the limit of massless external fermions, that all expressions are valid for u and v spinors, whose notation we unify as w in the remainder of this section. Furthermore, we reproduce here important identities of γ -matrices which are frequently used in the following. This is the case of the so-called Gordon identity

$$\begin{aligned} \gamma^\mu \gamma^\nu &= \frac{1}{2} \{ \gamma^\mu, \gamma^\nu \} + \frac{1}{2} [\gamma^\mu, \gamma^\nu] \\ &= g^{\mu\nu} - i \sigma^{\mu\nu} = g^{\mu\nu} + i \sigma^{\nu\mu}. \end{aligned} \quad (76)$$

A less common but nevertheless extremely useful identity is

$$\gamma^\mu \gamma^\rho \gamma^\nu = g^{\mu\rho} \gamma^\nu - g^{\mu\nu} \gamma^\rho + g^{\rho\nu} \gamma^\mu - i \varepsilon^{\mu\rho\nu\alpha} \gamma_\alpha \gamma_5, \quad (77)$$

with the Levi-Civita tensor $\varepsilon_{0123} = 1$ and $\gamma_5 = \frac{i}{4} \varepsilon_{\alpha\beta\mu\nu} \gamma^\alpha \gamma^\beta \gamma^\mu \gamma^\nu$. Based on this identity one can show several useful identities of four-fermion current products, first derived in [118]. We reproduce here its main results (Eqs. (1)-(4) of [118])

$$[\bar{w}_3 \gamma^\mu \gamma^\rho \gamma^\nu P_{L,R} w_1] [\bar{w}_4 \gamma_\mu \gamma^\tau \gamma_\nu P_{L,R} w_2] = 4 g^{\rho\tau} [\bar{w}_3 \gamma^\lambda P_{L,R} w_1] [\bar{w}_4 \gamma_\lambda P_{L,R} w_2], \quad (78)$$

$$[\bar{w}_3 \gamma^\mu \gamma^\rho \gamma^\nu P_{L,R} w_1] [\bar{w}_4 \gamma_\mu \gamma^\tau \gamma_\nu P_{R,L} w_2] = 4 [\bar{w}_3 \gamma^\tau P_{L,R} w_1] [\bar{w}_4 \gamma^\rho P_{R,L} w_2], \quad (79)$$

$$[\bar{w}_3 \gamma^\nu \gamma^\rho \gamma^\mu P_{L,R} w_1] [\bar{w}_4 \gamma_\mu \gamma^\tau \gamma_\nu P_{L,R} w_2] = 4 [\bar{w}_3 \gamma^\tau P_{L,R} w_1] [\bar{w}_4 \gamma^\rho P_{L,R} w_2], \quad (80)$$

$$[\bar{w}_3 \gamma^\nu \gamma^\rho \gamma^\mu P_{L,R} w_1] [\bar{w}_4 \gamma_\mu \gamma^\tau \gamma_\nu P_{R,L} w_2] = 4 g^{\rho\tau} [\bar{w}_3 \gamma^\lambda P_{L,R} w_1] [\bar{w}_4 \gamma_\lambda P_{R,L} w_2]. \quad (81)$$

Another very useful identity appears in a footnote of [118] and is given by

$$[\bar{w}_3 \gamma^\mu \gamma^\nu P_{L,R} w_1] [\bar{w}_4 \gamma_\mu \gamma_\nu P_{R,L} w_2] = 4 [\bar{w}_3 P_{L,R} w_1] [\bar{w}_4 P_{R,L} w_2]. \quad (82)$$

So far, the only condition used is that the dimensionality of spacetime is $D = 4$, meaning that these identities are valid independent of external fermion masses.

Let us then begin with the first two identities in Eqs. (67) and (68): one first makes use of the identity in Eq. (80) to obtain

$$p_2^\alpha p_1^\beta [\bar{w}_1 \gamma_\alpha P_L w_3] [\bar{w}_4 \gamma_\beta P_L w_2] = \frac{p_2^\alpha p_1^\beta}{4} [\bar{w}_1 \gamma^\nu \gamma_\beta \gamma^\mu P_L w_3] [\bar{w}_4 \gamma_\mu \gamma_\alpha \gamma_\nu P_L w_2]. \quad (83)$$

Although appearing significantly more complicated at first glance, we can anti-commute γ_β to the left-most and γ_α to the right-most position and apply the (massless) equations of motion, $\bar{w}_1 p_1 = 0$ and $p_2 w_2 = 0$, which lead us directly to

$$\frac{p_2^\alpha p_1^\beta}{4} [\bar{w}_1 (-\gamma_\beta \gamma^\nu + 2 g_\beta^\nu) \gamma^\mu P_L w_3] [\bar{w}_4 \gamma_\mu (-\gamma_\nu \gamma_\alpha + 2 g_{\alpha\nu}) P_L w_2] =$$

⁶Similar identities were obtained in [117].

$$= \frac{p_2^\alpha p_1^\beta}{4} \cdot 2 \cdot 2 \cdot g_{\alpha\nu} g_\beta^\nu [\bar{w}_1 \gamma^\mu P_L w_3] [\bar{w}_4 \gamma_\mu P_L w_2]. \quad (84)$$

The main focus here is to notice that in the left Dirac bracket we had a “slashed momentum” (which we could only annihilate in the right Dirac bracket) and vice-versa. With the help of Eq. (80) one switches the externally contracted γ -matrices between Dirac brackets thus enabling these simplifications.

In the same spirit one can derive the identities shown in Eqs. (72) and (73), albeit in a significantly more complicated way. First of all, one notices in the derivation of Eqs. (78-81), see [118] for details, that one can insert an additional γ -matrix completely to the left or right in each of the brackets; after a straight-forward computation (closely following [118]), one is led to

$$[\bar{w}_3 \gamma^\alpha \gamma^\mu \gamma^\rho \gamma^\nu P_{L,R} w_1] [\bar{w}_4 \gamma_\alpha \gamma_\mu \gamma^\tau \gamma_\nu P_{L,R} w_2] = 4g^{\rho\tau} [\bar{w}_3 \gamma^\alpha \gamma^\lambda P_{L,R} w_1] [\bar{w}_4 \gamma_\alpha \gamma_\lambda P_{L,R} w_2], \quad (85)$$

$$[\bar{w}_3 \gamma^\alpha \gamma^\mu \gamma^\rho \gamma^\nu P_{L,R} w_1] [\bar{w}_4 \gamma_\alpha \gamma_\mu \gamma^\tau \gamma_\nu P_{R,L} w_2] = 4[\bar{w}_3 \gamma^\alpha \gamma^\tau P_{L,R} w_1] [\bar{w}_4 \gamma_\alpha \gamma^\rho P_{R,L} w_2], \quad (86)$$

$$[\bar{w}_3 \gamma^\alpha \gamma^\nu \gamma^\rho \gamma^\mu P_{L,R} w_1] [\bar{w}_4 \gamma_\alpha \gamma_\mu \gamma^\tau \gamma_\nu P_{L,R} w_2] = 4[\bar{w}_3 \gamma^\alpha \gamma^\tau P_{L,R} w_1] [\bar{w}_4 \gamma_\alpha \gamma^\rho P_{L,R} w_2], \quad (87)$$

$$[\bar{w}_3 \gamma^\alpha \gamma^\nu \gamma^\rho \gamma^\mu P_{L,R} w_1] [\bar{w}_4 \gamma_\alpha \gamma_\mu \gamma^\tau \gamma_\nu P_{R,L} w_2] = 4g^{\rho\tau} [\bar{w}_3 \gamma^\alpha \gamma^\lambda P_{L,R} w_1] [\bar{w}_4 \gamma_\alpha \gamma_\lambda P_{R,L} w_2]. \quad (88)$$

Starting from the left-hand side of Eq. (69), we can first insert the Gordon identity and apply the equations of motion to obtain

$$A \equiv p_3^\alpha p_1^\beta [\bar{w}_1 \sigma_{\mu\alpha} P_{R} w_4] [\bar{w}_3 \sigma^\mu_\beta P_{L} w_2] = -p_3^\alpha p_1^\beta (g_{\alpha\beta} S_{RL} + [\bar{w}_1 \gamma^\mu \gamma_\alpha P_{R} w_4] [\bar{w}_3 \gamma_\mu \gamma_\beta P_{L} w_2]). \quad (89)$$

In the next step, we use the identity in Eq. (86) to rewrite the last second term of Eq. (89), giving us

$$\tilde{A} \equiv p_3^\alpha p_1^\beta [\bar{w}_1 \gamma^\mu \gamma_\alpha P_{R} w_4] [\bar{w}_3 \gamma_\mu \gamma_\beta P_{L} w_2] = \frac{p_3^\alpha p_1^\beta}{4} [\bar{w}_1 \gamma^\lambda \gamma^\mu \gamma_\beta \gamma^\nu P_{R} w_4] [\bar{w}_3 \gamma_\lambda \gamma_\mu \gamma_\alpha \gamma_\nu P_{L} w_2]. \quad (90)$$

Now one again anti-commutes γ_α and γ_β to the left-most slots and apply the equations of motion, leading to

$$\tilde{A} = p_3^\alpha p_1^\beta (8g_{\alpha\beta} S_{RL} - 2[\bar{w}_1 \gamma_\alpha \gamma^\nu P_{R} w_4] [\bar{w}_3 \gamma_\beta \gamma_\nu P_{L} w_2]). \quad (91)$$

Although the gain may not seem apparent, note the different order of γ -matrices in the second bracket. At this point one re-inserts the Gordon identity (this time the third equality of Eq.(76)) which gives us back the original term A as

$$\tilde{A} = p_3^\alpha p_1^\beta (2g_{\alpha\beta} S_{RL} + 2A), \quad (92)$$

such that finally we have

$$A = -p_3^\alpha p_1^\beta (g_{\alpha\beta} S_{RL} + 2g_{\alpha\beta} S_{RL} + 2A), \quad (93)$$

$$\Rightarrow A = -p_3^\alpha p_1^\beta g_{\alpha\beta} S_{RL}. \quad (94)$$

(Leading to the obtention of this result one can also quickly show Eqs.(73) by inserting once again the Gordon identity.)

The identity in Eq.(70) is probably the most cumbersome and the least evident: firstly, one notices that in deriving Eq.(69) both momenta had to be annihilated to the left of the brackets, while now we have one to the right and one to the left. One possible way to overcome this is to use the momentum conservation $p_1 + p_2 = p_3 + p_4$ to rewrite $p_2 = p_3 + p_4 - p_1$, so that one quickly shows that

$$[\bar{w}_1 \sigma_{\mu\alpha} P_{R} w_4] [\bar{w}_3 \sigma^\mu_\beta P_{L} w_2] p_1^\alpha p_1^\beta = 0, \quad (95)$$

again by inserting, the Gordon identity and using the fact that $\not{p}_1 \not{p}_1 = p_1^2 = 0$. Similarly, one can derive and use Eq. (71), which after insertion of the Gordon identity and $p_4 = p_1 + p_2 - p_3$ reduces to

$$[\bar{w}_1 P_{R} w_4] [\bar{w}_3 \sigma_{\alpha\beta} P_{L} w_2] p_4^\alpha p_1^\beta = ig_{\alpha\beta} (p_2^\alpha + p_3^\alpha) p_1^\beta S_{RL}. \quad (96)$$

Adding this term to our result of Eq. (69), we obtain Eq. (70). The remaining identities of Eqs. (73) and (74) can be derived by once again inserting the Gordon identity and applying the equations of motion.

Following the derivations in this appendix, more identities can be obtained in the limit of massless external fermions. For massive fermions the expressions become significantly more complicated and are left for future work should external fermion masses become relevant.

References

- [1] P. Minkowski, $\mu \rightarrow e\gamma$ at a Rate of One Out of 10^9 Muon Decays?, *Phys. Lett. B* **67** (1977) 421.
- [2] T. Yanagida, Horizontal gauge symmetry and masses of neutrinos, *Conf. Proc. C* **7902131** (1979) 95.
- [3] S.L. Glashow, The Future of Elementary Particle Physics, *NATO Sci. Ser. B* **61** (1980) 687.
- [4] M. Gell-Mann, P. Ramond and R. Slansky, Complex Spinors and Unified Theories, *Conf. Proc. C* **790927** (1979) 315 [[1306.4669](#)].
- [5] R.N. Mohapatra and G. Senjanovic, Neutrino Mass and Spontaneous Parity Nonconservation, *Phys. Rev. Lett.* **44** (1980) 912.
- [6] E.K. Akhmedov, M. Lindner, E. Schnapka and J.W.F. Valle, Dynamical left-right symmetry breaking, *Phys. Rev. D* **53** (1996) 2752 [[hep-ph/9509255](#)].
- [7] M. Malinsky, J.C. Romao and J.W.F. Valle, Novel supersymmetric $SO(10)$ seesaw mechanism, *Phys. Rev. Lett.* **95** (2005) 161801 [[hep-ph/0506296](#)].
- [8] J. Schechter and J.W.F. Valle, Neutrino Masses in $SU(2) \times U(1)$ Theories, *Phys. Rev. D* **22** (1980) 2227.
- [9] M. Gronau, C.N. Leung and J.L. Rosner, Extending Limits on Neutral Heavy Leptons, *Phys. Rev. D* **29** (1984) 2539.
- [10] R.N. Mohapatra and J.W.F. Valle, Neutrino Mass and Baryon Number Nonconservation in Superstring Models, *Phys. Rev. D* **34** (1986) 1642.
- [11] T. Riemann and G. Mann, NONDIAGONAL Z DECAY: $Z \rightarrow E \text{ MU}$, in 10th International Conference on Neutrino Physics: Neutrino '82, pp. 58–61, 1982.
- [12] J.I. Illana, M. Jack and T. Riemann, Predictions for $Z \rightarrow \mu \text{ tau}$ and related reactions, [hep-ph/0001273](#).
- [13] G. Mann and T. Riemann, EFFECTIVE FLAVOR CHANGING WEAK NEUTRAL CURRENT IN THE STANDARD THEORY AND Z BOSON DECAY, *Annalen Phys.* **40** (1984) 334.
- [14] J.I. Illana and T. Riemann, Charged lepton flavor violation from massive neutrinos in Z decays, *Phys. Rev. D* **63** (2001) 053004 [[hep-ph/0010193](#)].
- [15] R. Alonso, M. Dhen, M.B. Gavela and T. Hambye, Muon conversion to electron in nuclei in type-I seesaw models, *JHEP* **01** (2013) 118 [[1209.2679](#)].
- [16] A. Ilakovac and A. Pilaftsis, Flavor violating charged lepton decays in seesaw-type models, *Nucl. Phys. B* **437** (1995) 491 [[hep-ph/9403398](#)].
- [17] E. Ma and A. Pramudita, Flavor Changing Effective Neutral Current Couplings in the Weinberg-Salam Model, *Phys. Rev. D* **22** (1980) 214.
- [18] F. Deppisch and J.W.F. Valle, Enhanced lepton flavor violation in the supersymmetric inverse seesaw model, *Phys. Rev. D* **72** (2005) 036001 [[hep-ph/0406040](#)].
- [19] F. Deppisch, T.S. Kosmas and J.W.F. Valle, Enhanced $\mu - e$ conversion in nuclei in the inverse seesaw model, *Nucl. Phys. B* **752** (2006) 80 [[hep-ph/0512360](#)].
- [20] D.N. Dinh, A. Ibarra, E. Molinaro and S.T. Petcov, The $\mu - e$ Conversion in Nuclei, $\mu \rightarrow e\gamma$, $\mu \rightarrow 3e$ Decays and TeV Scale See-Saw Scenarios of Neutrino Mass Generation, *JHEP* **08** (2012) 125 [[1205.4671](#)].
- [21] T. Hambye, CLFV and the origin of neutrino masses, *Nucl. Phys. B Proc. Suppl.* **248-250** (2014) 13 [[1312.5214](#)].
- [22] A. Abada, M.E. Krauss, W. Porod, F. Staub, A. Vicente and C. Weiland, Lepton flavor violation in low-scale seesaw models: SUSY and non-SUSY contributions, *JHEP* **11** (2014) 048 [[1408.0138](#)].
- [23] A. Abada, V. De Romeri and A.M. Teixeira, Impact of sterile neutrinos on nuclear-assisted cLFV processes, *JHEP* **02** (2016) 083 [[1510.06657](#)].
- [24] A. Abada, D. Bećirević, M. Lucente and O. Sumensari, Lepton flavor violating decays of vector quarkonia and of the Z boson, *Phys. Rev. D* **91** (2015) 113013 [[1503.04159](#)].
- [25] A. Abada, V. De Romeri, J. Orloff and A.M. Teixeira, In-flight cLFV conversion: $e - \mu$, $e - \tau$ and $\mu - \tau$ in minimal extensions of the standard model with sterile fermions, *Eur. Phys. J. C* **77** (2017) 304 [[1612.05548](#)].

[26] L. Calibbi and G. Signorelli, *Charged Lepton Flavour Violation: An Experimental and Theoretical Introduction*, *Riv. Nuovo Cim.* **41** (2018) 71 [1709.00294].

[27] A. Abada and A.M. Teixeira, *Heavy neutral leptons and high-intensity observables*, *Front. in Phys.* **6** (2018) 142 [1812.08062].

[28] E. Arganda, M.J. Herrero, X. Marcano and C. Weiland, *Imprints of massive inverse seesaw model neutrinos in lepton flavor violating Higgs boson decays*, *Phys. Rev. D* **91** (2015) 015001 [1405.4300].

[29] X. Marcano and R.A. Morales, *Flavor techniques for LFV processes: Higgs decays in a general seesaw model*, *Front. in Phys.* **7** (2020) 228 [1909.05888].

[30] K.A. Urquía-Calderón, I. Timiryasov and O. Ruchayskiy, *Heavy neutral leptons — Advancing into the PeV domain*, *JHEP* **08** (2023) 167 [2206.04540].

[31] FCC-EE STUDY TEAM collaboration, *Search for Heavy Right Handed Neutrinos at the FCC-ee*, *Nucl. Part. Phys. Proc.* **273-275** (2016) 1883 [1411.5230].

[32] S. Antusch, E. Cazzato and O. Fischer, *Sterile neutrino searches at future e^-e^+ , pp , and e^-p colliders*, *Int. J. Mod. Phys. A* **32** (2017) 1750078 [1612.02728].

[33] Y. Cai, T. Han, T. Li and R. Ruiz, *Lepton Number Violation: Seesaw Models and Their Collider Tests*, *Front. in Phys.* **6** (2018) 40 [1711.02180].

[34] A. Blondel et al., *Searches for long-lived particles at the future FCC-ee*, *Front. in Phys.* **10** (2022) 967881 [2203.05502].

[35] A.M. Abdullahi et al., *The present and future status of heavy neutral leptons*, *J. Phys. G* **50** (2023) 020501 [2203.08039].

[36] A. Abada, P. Escribano, X. Marcano and G. Piazza, *Collider searches for heavy neutral leptons: beyond simplified scenarios*, *Eur. Phys. J. C* **82** (2022) 1030 [2208.13882].

[37] P. Giffin, S. Gori, Y.-D. Tsai and D. Tuckler, *Heavy neutral leptons at beam dump experiments of future lepton colliders*, *JHEP* **04** (2023) 046 [2206.13745].

[38] M. Drewes, *Distinguishing Dirac and Majorana Heavy Neutrinos at Lepton Colliders*, *PoS ICHEP2022* (2022) 608 [2210.17110].

[39] M. Ovchynnikov and J.-Y. Zhu, *Search for the dipole portal of heavy neutral leptons at future colliders*, *JHEP* **07** (2023) 039 [2301.08592].

[40] S. Ajmal, P. Azzi, S. Giappichini, M. Klute, O. Panella, M. Presilla et al., *Searching for type I seesaw mechanism in a two Heavy Neutral Leptons scenario at FCC-ee*, 2410.03615.

[41] S. Antusch, J. Hajar and B.M.S. Oliveira, *Discovering heavy neutrino-antineutrino oscillations at the Z-pole*, *JHEP* **11** (2024) 102 [2408.01389].

[42] I. Chakraborty, H. Roy and T. Srivastava, *Searches for heavy neutrinos at multi-TeV muon collider: a resonant leptogenesis perspective*, *Eur. Phys. J. C* **83** (2023) 280 [2206.07037].

[43] K. Mękała, J. Reuter and A.F. Żarnecki, *Optimal search reach for heavy neutral leptons at a muon collider*, *Phys. Lett. B* **841** (2023) 137945 [2301.02602].

[44] T.H. Kwok, L. Li, T. Liu and A. Rock, *Searching for heavy neutral leptons at a future muon collider*, *Phys. Rev. D* **110** (2024) 075009 [2301.05177].

[45] P. Li, Z. Liu and K.-F. Lyu, *Heavy neutral leptons at muon colliders*, *JHEP* **03** (2023) 231 [2301.07117].

[46] O. Mikulenko and M. Marinichenko, *Measuring lepton number violation in heavy neutral lepton decays at the future muon collider*, *JHEP* **01** (2024) 032 [2309.16837].

[47] K.A. Urquía-Calderón, *Long-lived heavy neutral leptons at lepton colliders as a probe of left-right-symmetric models*, *Phys. Rev. D* **109** (2024) 055002 [2310.17406].

[48] C.H. de Lima, D. McKeen, J.N. Ng, M. Shamma and D. Tuckler, *Probing Lepton Number Violation at Same-Sign Lepton Colliders*, 2411.15303.

[49] M.B. Marcos, A. de Giorgi, L. Merlo and J.-L. Tastet, *ALPs and HNLs at LHC and Muon Colliders: Uncovering New Couplings and Signals*, 2407.14970.

[50] Y. Hamada, R. Kitano, R. Matsudo, H. Takaura and M. Yoshida, *μ TRISTAN*, *PTEP* **2022** (2022) 053B02 [2201.06664].

[51] M. Lu, A.M. Levin, C. Li, A. Agapitos, Q. Li, F. Meng et al., *The physics case for an electron-muon collider*, *Adv. High Energy Phys.* **2021** (2021) 6693618 [2010.15144].

[52] F. Bossi and P. Ciafaloni, *Lepton Flavor Violation at muon-electron colliders*, *JHEP* **10** (2020) 033 [2003.03997].

[53] J. Kriewald, J. Orloff, E. Pinsard and A.M. Teixeira, *Prospects for a flavour violating Z' explanation of $\Delta a_{\mu,e}$* , *Eur. Phys. J. C* **82** (2022) 844 [2204.13134].

[54] A. Goudelis, J. Kriewald, E. Pinsard and A.M. Teixeira, *cLFV leptophilic Z' as a dark matter portal: prospects for colliders*, *Eur. Phys. J. C* **84** (2024) 804 [2312.14103].

[55] P.S.B. Dev, J. Heeck and A. Thapa, *Neutrino mass models at μ TRISTAN*, *Eur. Phys. J. C* **84** (2024) 148 [2309.06463].

[56] P.D. Bolton, J. Kriewald, M. Nemevšek, F. Nesti and J.C. Vasquez, *On Lepton Number Violation in the Type II Seesaw*, 2408.00833.

[57] A. Das, J. Li, S. Mandal, T. Nomura and R. Zhang, *Testing tree level TeV scale type-I and type-II seesaw scenarios in μ TRISTAN*, 2410.21956.

[58] Y. Kondo et al., *Re-Acceleration of Ultra Cold Muon in J-PARC Muon Facility*, in *9th International Particle Accelerator Conference*, 6, 2018, DOI.

[59] M. Abe et al., *A New Approach for Measuring the Muon Anomalous Magnetic Moment and Electric Dipole Moment*, *PTEP* **2019** (2019) 053C02 [1901.03047].

[60] C. Adolphsen et al., eds., *The International Linear Collider Technical Design Report - Volume 3.I: Accelerator \& in the Technical Design Phase*, 1306.6353.

[61] FCC collaboration, *FCC-ee: The Lepton Collider: Future Circular Collider Conceptual Design Report Volume 2*, *Eur. Phys. J. ST* **228** (2019) 261.

[62] CEPC STUDY GROUP collaboration, *CEPC Conceptual Design Report: Volume 1 - Accelerator*, 1809.00285.

[63] Y. Hamada, R. Kitano, R. Matsudo and H. Takaoka, *Precision $\mu+\mu+$ and $\mu+e-$ elastic scatterings*, *PTEP* **2023** (2023) 013B07 [2210.11083].

[64] T. Hahn and M. Perez-Victoria, *Automatized one loop calculations in four-dimensions and D-dimensions*, *Comput. Phys. Commun.* **118** (1999) 153 [hep-ph/9807565].

[65] A. Abada, J. Kriewald, E. Pinsard, S. Rosauro-Alcaraz and A.M. Teixeira, *LFV Higgs and Z -boson decays: leptonic CPV phases and CP asymmetries*, *Eur. Phys. J. C* **83** (2023) 494 [2207.10109].

[66] J. Brod and M. Gorbahn, *The Z Penguin in Generic Extensions of the Standard Model*, *JHEP* **09** (2019) 027 [1903.05116].

[67] A. Denner, H. Eck, O. Hahn and J. Kublbeck, *Feynman rules for fermion number violating interactions*, *Nucl. Phys. B* **387** (1992) 467.

[68] J.F. Nieves and P.B. Pal, *Generalized Fierz identities*, *Am. J. Phys.* **72** (2004) 1100 [hep-ph/0306087].

[69] A. Abada and T. Toma, *Electric Dipole Moments of Charged Leptons with Sterile Fermions*, *JHEP* **02** (2016) 174 [1511.03265].

[70] A. Abada, J. Kriewald and A.M. Teixeira, *On the role of leptonic CPV phases in cLFV observables*, *Eur. Phys. J. C* **81** (2021) 1016 [2107.06313].

[71] I. Esteban, M.C. Gonzalez-Garcia, M. Maltoni, I. Martinez-Soler, J.a.P. Pinheiro and T. Schwetz, *NuFit-6.0: Updated global analysis of three-flavor neutrino oscillations*, 2410.05380.

[72] P.S.B. Dev and A. Pilaftsis, *Minimal Radiative Neutrino Mass Mechanism for Inverse Seesaw Models*, *Phys. Rev. D* **86** (2012) 113001 [1209.4051].

[73] G. 't Hooft, C. Itzykson, A. Jaffe, H. Lehmann, P.K. Mitter, I.M. Singer et al., *Recent Developments in Gauge Theories. Proceedings, Nato Advanced Study Institute, Cargese, France, August 26 - September 8, 1979*, vol. 59, pp. pp.1-438, 1980, DOI.

[74] H. Hettmansperger, M. Lindner and W. Rodejohann, *Phenomenological Consequences of sub-leading Terms in See-Saw Formulas*, *JHEP* **04** (2011) 123 [1102.3432].

[75] A. Abada and M. Luente, *Looking for the minimal inverse seesaw realisation*, *Nucl. Phys. B* **885** (2014) 651 [1401.1507].

[76] J.A. Casas and A. Ibarra, *Oscillating neutrinos and $\mu \rightarrow e, \gamma$* , *Nucl. Phys. B* **618** (2001) 171 [[hep-ph/0103065](#)].

[77] K.A. Urquía-Calderón, I. Timiryasov and O. Ruchayskiy, *Bounds on heavy neutral leptons from tree level unitarity*, [2409.13412](#).

[78] M.S. Chanowitz, M.A. Furman and I. Hinchliffe, *Weak Interactions of Ultraheavy Fermions. 2.*, *Nucl. Phys. B* **153** (1979) 402.

[79] L. Durand, J.M. Johnson and J.L. Lopez, *Perturbative Unitarity Revisited: A New Upper Bound on the Higgs Boson Mass*, *Phys. Rev. Lett.* **64** (1990) 1215.

[80] J. Bernabeu, J.G. Korner, A. Pilaftsis and K. Schilcher, *Universality breaking effects in leptonic Z decays*, *Phys. Rev. Lett.* **71** (1993) 2695 [[hep-ph/9307295](#)].

[81] S. Fajfer and A. Ilakovac, *Lepton flavor violation in light hadron decays*, *Phys. Rev. D* **57** (1998) 4219.

[82] A. Ilakovac, *Lepton flavor violation in the standard model extended by heavy singlet Dirac neutrinos*, *Phys. Rev. D* **62** (2000) 036010 [[hep-ph/9910213](#)].

[83] A. Abada, J. Kriewald, E. Pinsard, S. Rosauro-Alcaraz and A.M. Teixeira, *Heavy neutral lepton corrections to SM boson decays: lepton flavour universality violation in low-scale seesaw realisations*, *Eur. Phys. J. C* **84** (2024) 149 [[2307.02558](#)].

[84] E. Fernandez-Martinez, M.B. Gavela, J. Lopez-Pavon and O. Yasuda, *CP-violation from non-unitary leptonic mixing*, *Phys. Lett. B* **649** (2007) 427 [[hep-ph/0703098](#)].

[85] E. Fernandez-Martinez, J. Hernandez-Garcia, J. Lopez-Pavon and M. Luente, *Loop level constraints on Seesaw neutrino mixing*, *JHEP* **10** (2015) 130 [[1508.03051](#)].

[86] E. Fernandez-Martinez, J. Hernandez-Garcia and J. Lopez-Pavon, *Global constraints on heavy neutrino mixing*, *JHEP* **08** (2016) 033 [[1605.08774](#)].

[87] M. Blennow, E. Fernández-Martínez, J. Hernández-García, J. López-Pavón, X. Marcano and D. Naredo-Tuero, *Bounds on lepton non-unitarity and heavy neutrino mixing*, *JHEP* **08** (2023) 030 [[2306.01040](#)].

[88] A. Abada, J. Kriewald, E. Pinsard, S. Rosauro-Alcaraz and A.M. Teixeira, *LFV Higgs and Z-boson decays: leptonic CPV phases and CP asymmetries*, *Eur. Phys. J. C* **83** (2023) 494 [[2207.10109](#)].

[89] MEG II collaboration, *A search for $\mu^+ \rightarrow e^+ \gamma$ with the first dataset of the MEG II experiment*, *Eur. Phys. J. C* **84** (2024) 216 [[2310.12614](#)].

[90] MEG II collaboration, *The design of the MEG II experiment*, *Eur. Phys. J. C* **78** (2018) 380 [[1801.04688](#)].

[91] BABAR collaboration, *Searches for Lepton Flavor Violation in the Decays $\tau^{+-} \rightarrow e^{+-} \gamma$ and $\tau^{+-} \rightarrow \mu^{+-} \gamma$* , *Phys. Rev. Lett.* **104** (2010) 021802 [[0908.2381](#)].

[92] BELLE-II collaboration, *The Belle II Physics Book*, *PTEP* **2019** (2019) 123C01 [[1808.10567](#)].

[93] BELLE collaboration, *Search for lepton-flavor-violating tau-lepton decays to $\ell\gamma$ at Belle*, *JHEP* **10** (2021) 19 [[2103.12994](#)].

[94] SINDRUM collaboration, *Search for the Decay $\mu^+ \rightarrow e^+ e^+ e^-$* , *Nucl. Phys. B* **299** (1988) 1.

[95] A. Blondel et al., *Research Proposal for an Experiment to Search for the Decay $\mu \rightarrow eee$* , [1301.6113](#).

[96] K. Hayasaka et al., *Search for Lepton Flavor Violating Tau Decays into Three Leptons with 719 Million Produced Tau+Tau- Pairs*, *Phys. Lett. B* **687** (2010) 139 [[1001.3221](#)].

[97] BELLE-II collaboration, *Search for lepton-flavor-violating $\tau^- \rightarrow \mu^- \mu^+ \mu^-$ decays at Belle II*, *JHEP* **09** (2024) 062 [[2405.07386](#)].

[98] FCC collaboration, *FCC Physics Opportunities: Future Circular Collider Conceptual Design Report Volume 1*, *Eur. Phys. J. C* **79** (2019) 474.

[99] SINDRUM II collaboration, *A Search for muon to electron conversion in muonic gold*, *Eur. Phys. J. C* **47** (2006) 337.

[100] DEEME collaboration, *Search for $\mu - e$ conversion with DeeMe experiment at J-PARC MLF*, *PoS FPCP2015* (2015) 060.

[101] COMET collaboration, *An Overview of the COMET Experiment and its Recent Progress*, in *17th International Workshop on Neutrino Factories and Future Neutrino Facilities*, 12, 2015 [1512.08564].

[102] COMET collaboration, *COMET Phase-I Technical Design Report*, *PTEP* **2020** (2020) 033C01 [1812.09018].

[103] COMET collaboration, *Search for Muon-to-Electron Conversion with the COMET Experiment*, *J. Universe* **8** (2022) 196 [2203.06365].

[104] Mu2E collaboration, *Mu2e Technical Design Report*, 1501.05241.

[105] L. Willmann et al., *New bounds from searching for muonium to anti-muonium conversion*, *Phys. Rev. Lett.* **82** (1999) 49 [hep-ex/9807011].

[106] A.-Y. Bai et al., *Conceptual Design of the Muonium-to-Antimuonium Conversion Experiment (MACE)*, 2410.18817.

[107] ATLAS collaboration, *Search for the lepton flavor violating decay $Z \rightarrow e\mu$ in pp collisions at \sqrt{s} TeV with the ATLAS detector*, *Phys. Rev. D* **90** (2014) 072010 [1408.5774].

[108] ATLAS collaboration, *Search for lepton-flavor-violation in Z -boson decays with τ -leptons with the ATLAS detector*, *Phys. Rev. Lett.* **127** (2022) 271801 [2105.12491].

[109] A. Abada, A.M. Teixeira, A. Vicente and C. Weiland, *Sterile neutrinos in leptonic and semileptonic decays*, *JHEP* **02** (2014) 091 [1311.2830].

[110] A. Abada, D. Das, A.M. Teixeira, A. Vicente and C. Weiland, *Tree-level lepton universality violation in the presence of sterile neutrinos: impact for R_K and R_π* , *JHEP* **02** (2013) 048 [1211.3052].

[111] ATLAS collaboration, *Technical Design Report for the ATLAS Inner Tracker Pixel Detector*, 2017. 10.17181/CERN.FOZZ.ZP3Q.

[112] ATLAS collaboration, *Search for high-mass resonances in final states with a τ -lepton and missing transverse momentum with the ATLAS detector*, *Phys. Rev. D* **109** (2024) 112008 [2402.16576].

[113] H.H. Patel, *Package-X: A Mathematica package for the analytic calculation of one-loop integrals*, *Comput. Phys. Commun.* **197** (2015) 276 [1503.01469].

[114] V. Shtabovenko, R. Mertig and F. Orellana, *New Developments in FeynCalc 9.0*, *Comput. Phys. Commun.* **207** (2016) 432 [1601.01167].

[115] V. Shtabovenko, R. Mertig and F. Orellana, *FeynCalc 9.3: New features and improvements*, *Comput. Phys. Commun.* **256** (2020) 107478 [2001.04407].

[116] V. Shtabovenko, R. Mertig and F. Orellana, *FeynCalc 10: Do multiloop integrals dream of computer codes?*, *Comput. Phys. Commun.* **306** (2025) 109357 [2312.14089].

[117] J.L.G. Santiago, D. Portillo-Sánchez, G. Hernández-Tomé and J. Rendón, *Authentic Majorana versus singlet Dirac neutrino contributions to $\mu + \mu \rightarrow \ell + \ell$ ($\ell = e, \tau$) transitions*, *Phys. Rev. D* **110** (2024) 053006 [2405.02819].

[118] A. Sirlin, *A Class of Useful Identities Involving Correlated Direct Products of γ Matrices*, *Nucl. Phys. B* **192** (1981) 93.